EUROPEAN ORGANIZATION FOR NUCLEAR RESEARCH

CERN-EP/87-192
9 October 1987

THREE-JET EVENTS AT THE CERN INTERSECTING STORAGE RINGS

CERN[1] – Michigan State[2] – Oxford[3] – Rockefeller[4] (CMOR) Collaboration

A.L.S. Angelis [3,*)], G. Basini [1,**)], H.-J. Besch [1,***)], R.E. Breedon [4)], L. Camilleri [1)], T.J. Chapin [4)], R.L. Cool [4)], P.T. Cox [1,4)], C. von Gagern [1,4,†)], C. Grosso-Pilcher [1,††)], D.S. Hanna [1,4,†††)], B.M. Humphries [2)], J.T. Linnemann [2,4)], C. Newman-Holmes [1,#)], R.B. Nickerson [3,##)], N. Phinney [1,3,###)], B.G. Pope [2)], S.H. Pordes [1,4,#)], K.J. Powell [3)], R.W. Rusack [4)], C.W. Salgado [2)], A.M. Segar [3)], S.R. Stampke [2,+)], M.J. Tannenbaum [4,++)] and J.M. Yelton [3)]

Abstract

Three-jet events have been observed in pp collisions at $\sqrt{s} = 62.3$ GeV. The data were collected using a total neutral energy trigger with a threshold at 25 GeV. These events appear predominantly as two jets, with some appearing as three jets. A novel analysis for the extraction of 2-jet and 3-jet events is described, and some of the event properties are discussed. The relative numbers of two- and three-jet events are studied within the framework of leading-order QCD, and yield a value of $\alpha_S(K_3/K_2) = 0.19 \pm 0.02$ (stat.) $\pm$ 0.04 (syst.).

[Submitted to Nucl. Phys. B – 30.09.87]

---

1) CERN, CH-1211 Geneva 23, Switzerland
2) Dept. of Physics & Astronomy, Michigan State University, East Lansing, MI 48824, USA
3) Dept. of Physics, Oxford University, Oxford, UK
4) Experimental Physics Dept., The Rockefeller University, New York, NY 10021, USA

*) Present address: University College London, London, UK
**) Present address: Laboratori Nazionali dell' INFN, Frascati, Italy
***) Present address: Universität – GHS, Siegen, West Germany
†) Present address: Rohde & Schwarz, Munich, West Germany
††) Present address: Enrico Fermi Institute, University of Chicago, Chicago, IL, USA
†††) Present address: McGill University, Montreal, Quebec, Canada
#) Present address: FNAL, Batavia, IL, USA
##) Present address: Harvard University, Cambridge, MA, USA
###) Present address: SLAC, Stanford, CA, USA
+) Present address: University of Notre Dame, IN, USA
++) Present address: BNL, Upton, NY, USA

1. Introduction

Although considerable data have been amassed concerning 2-jet production in hadron-hadron collisions at high transverse energies, little has yet been presented on 3-jet events. Such events were first observed at the CERN Intersecting Storage Rings (ISR) at a centre-of-mass (c.m.) energy $\sqrt{s}$ = 62 GeV [1]. Three-jet events in e^+e^- interactions have of course been studied for several years [2] and recent results from the CERN SPS $\bar{p}p$ collider have shown the emergence of very clear 2-jet [3] and 3-jet [4,5] events in hadron collisions at $\sqrt{s}$ = 540 and 630 GeV. In this paper results are presented from the analysis of events obtained by triggering on the energy deposition in an electromagnetic (e.m.) calorimeter covering 90% of 2π in azimuth in pp collisions at $\sqrt{s}$ = 62 GeV at the ISR. Two-jet results from this experiment, R110, have already been discussed [6,7].

Another ISR experiment has presented results on three jets [8] but based on a 3-jet trigger rather than the global energy trigger used here.

2. Apparatus and Trigger

The apparatus, trigger, and data-taking conditions have been discussed in refs. 6 and 7. Only the most important features will be reviewed here; fig. 1 shows the apparatus. Charged particles were detected, over the full azimuth, in a set of cylindrical drift chambers inside a superconducting solenoidal magnetic field, centred on the interaction region of the two proton beams in the ISR. Two arrays of lead glass outside the solenoid, at 90° to the colliding beam directions, were used to detect e.m. energy. Four modules of lead-scintillator shower counters, inside the solenoid, detected e.m. showers in the azimuthal range not covered by the lead glass arrays. The rapidity coverage was ± 0.6 units of rapidity in the pp c.m. system for the lead glass, ± 1.2 units for the shower counters, and ± 1.5 units for charged particles in the drift chambers. Signals from the phototubes viewing the lead glass blocks and the shower counters were summed and used as a trigger once this neutral energy exceeded a nominal threshold of 25 GeV. In the offline analysis more detailed calibration information was used, and only events for which the hardware trigger was fully efficient were retained for further study. Due to the unrestrictive nature of this trigger, and the high instantaneous luminosity of the ISR (typically 5×10^{31} $cm^{-2}s^{-1}$), over 90% of the triggers were due to the overlap of more than one interaction occurring

within the recording time of the apparatus, but these events were removed after examining the pattern of times of arrival of all phototube signals in each event [6]. Overlapping events are not involved in the analysis presented here. The total integrated luminosity for the data discussed was 6×10^{37} cm^{-2}, in pp collisions at $\sqrt{s} = 62.3$ GeV. About half of this sample was used to obtain the total neutral transverse energy spectrum and results on 2-jet physics presented in ref. 7.

3. Energy-flow analysis

3.1 Diagonalization of the sphericity tensor

It has been previously shown [6,7] that as the total energy in the events increases 2-jet events gradually come to dominate the event sample. In the present analysis we re-examine the structure of the events, by first studying the energy flow, and showing that events exist which have the structure expected of 3-jets, without forcing a jet-finding algorithm on the data. Then we apply a jet-finding algorithm to extract explicitly the multijet component of the data sample.

A 4-momentum vector, in the Laboratory frame, is calculated from each detected charged particle with a momentum above 300 MeV/c, and from each e.m. detector element containing energy above about 50 MeV/c (see ref. 6 for details). All momenta are first transformed into the event rest-frame calculated from all detected particles. The energy flow is examined relative to the sphericity axis of each event. For each event the sphericity tensor T is calculated as [9] :

$$T^{\alpha\beta} = \Sigma_i(\delta^{\alpha\beta}\,\vec{p}_i^{\,2} - p_i^{\alpha}p_i^{\beta})$$

where the sum (index i) is over all detected particles, and α and β label the three space components of each particle momentum $\vec{p}_i$. This tensor is diagonalized to obtain the eigenvalues λ_1, λ_2, λ_3 which are the sums of the squares of the transverse momenta with respect to the three eigenvector directions $\hat{n}_1$, $\hat{n}_2$, $\hat{n}_3$ respectively. The eigenvalues are ordered $\lambda_3 < \lambda_2 < \lambda_1$, so λ_3 is the minimum Σp_T^2 (w.r.t. $\hat{n}_3$), and λ_1 is the maximum Σp_T^2 (w.r.t. $\hat{n}_1$). The direction $\hat{n}_3$ defines the sphericity axis. From the λ_j three shape parameters Q_j are defined by

$$Q_j = 1 - 2\lambda_j/(\lambda_1+\lambda_2+\lambda_3),$$

in analogy with e^+e^- analyses [10]. These satisfy $Q_1 + Q_2 + Q_3 = 1$. Notice that the denominator of the second term is $2\Sigma\vec{p}_i^{\,2}$, since this is the trace of the tensor, so that $Q_j \sim \Sigma(\vec{p}_i \cdot \hat{n}_j)^2$, and thus Q_3 corresponds to the eigenvector $\hat{n}_3$ along which the sum of longitudinal momentum-squared in an event is maximized. Also, the sphericity S is defined as $3(\min \Sigma p_T^{\,2})/2(\Sigma\vec{p}^{\,2})$, which can be written in terms of the Q's as $3(1-Q_3)/2$. The event topology is now described by a point (Q_1,Q_2,Q_3) in a Dalitz plot representation [10], as indicated in fig. 2a).

3.2 Event structures

Events in which the energy-flow lies approximately in one plane (disk-shaped events) have $Q_1 \sim 0$, events in which the energy-flow is in two back-to-back cones (linear events) have both Q_1 and $Q_2 \sim 0$, and isotropic events have all three $Q_j \sim 1/3$. The scaled Dalitz plot, $(1.5Q_1,1.5Q_2,1.5Q_3)$, which is equivalent to a scatterplot of $(\sqrt{3}/2)(Q_2 - Q_1)$ against $(3/2)(Q_1 + Q_2)$ $(= S)$, is shown for our data in fig. 2b), and its projections are given in fig. 2c) and d) respectively. This Dalitz plot effectively summarizes the different event structures occurring in the data. The highest density of events is in the corner of high Q_3 (or equivalently, low S) and with both Q_1 and Q_2 low and approximately equal. Away from this corner the density rapidly decreases, although there are events lying in most of the physically-allowed region (the shaded region of fig. 2a)), except for that corresponding to perfectly isotropic events ($S \approx 1$, $Q_1 \approx Q_2 \approx Q_3$).

We proceed to examine the energy flow in various subsamples of the events, selected according to their particular sets of Q_j values.

3.3 Energy flow relative to the sphericity axis

The distribution of the energy flow relative to the sphericity axis is examined in the plane defined by the eigenvectors $\hat{n}_2$ and $\hat{n}_3$, using an azimuthal angle ϕ measured w.r.t that axis. Since the sphericity is quadratic in the momenta there is no a priori way to distinguish $\phi = 0$ from $\phi = 180°$. To make this choice we proceed as follows: In each of the hemispheres about the sphericity axis the transverse momentum, j_T, of each particle lying in that hemisphere is calculated relative to the axis. The average $< j_T^{\,2}/\sin\theta >$ is calculated over the particles within each hemisphere. (The $\sin\theta$ term compensates for the increased solid angle as the polar angle θ increases). The direction corresponding to the smaller average is taken as $\phi = 0$. In a 2-jet event this corresponds to the direction of the narrower jet. The

energy flow is plotted as $(1/E_{tot})(dE/d\phi)$, so that the integral of the distribution over ϕ gives the total number of events contributing to the plot.

The energy flow in the whole event sample is shown in fig. 3a). Note the tightness of the energy flow along the S axis: the dominant event-type is "2-jet-like". Selecting the most linear events by requiring Q_1 and Q_2 low (< 0.05) gives the energy flow shown in fig. 3b). The events of particular interest in a 3-jet search are those which are planar (i.e. Q_1 small) but with a broad recoil structure ($Q_2 - Q_1$ large). It is here that "3-jet-like" events would be expected to appear, since the otherwise overwhelming 2-jet structure has now been removed. The energy flow in such events is shown in Figure 3c), using the selection $Q_1 < 0.1$ and $(Q_2 - Q_1) > 0.1$. The flow no longer has two narrow lobes. There is a narrow distribution at 0°, but the broad recoil distribution shows a dip at 180°. This dip shows that the recoil distribution is not due to an isotropic distribution of particles but contains some events in which the recoil is composed of two distinct clusters of energy. Note that the size of the dip is large ($\sim 15°$) relative to the angular granularity of our detector ($< 6°$). Monte Carlo studies show that such a dip can also result from low-multiplicity effects since a two-particle recoil would necessarily give such a dip, although this effect is masked as soon as there are more than two particles. The dip is still seen if the sample is restricted to events in which the three most energetic particles in the recoil hemisphere contain less than 50% of the hemisphere energy (55% of the events). This result is insensitive to the precise values used to select the sample (both cuts were varied from 0.05 to 0.10). We shall return later to the energy-flow in reconstructed 3-jet events, which is shown in fig. 3d).

The Q_i cuts select only on the overall event topology, and not explicitly on the multiplicities of particles, clusters, or jets. The Monte Carlo studies also show that the Q_i cuts do not themselves enforce a dip, and that neither the acceptance of the detector nor the analysis procedure itself do either. The conclusion is that events with two clusters of energy in the recoil hemisphere are a dominant component of all planar events with a broad recoil structure: they are neither purely 2-jet-like nor isotropic.

4. Reconstruction of the jets

4.1 Introduction

In order to study jet properties some method of jet reconstruction must be used. The extraction of 3-jet events from hadron-hadron data is bedevilled by the fact that the third jet is usually buried within the particles of the other jets, especially at the relatively low $\sqrt{s}$ values available at the ISR, as well as by confusion from low p_T particles from spectator fragmentation (although these may be expected to be of high enough rapidity to fall outside the acceptance of our detector). There are, however, some events in which the separation between the three jets is sufficiently unambiguous that a suitably chosen jet-finding algorithm may be used to identify them. There is often a further complication in that data from several different types of detector must be analysed together.

The algorithm used here was developed from the approach suggested by Donati et al. [11] which involves Fourier analysis, and subsequent digital filtering, of the energy flow in the events. This method proved to be simple and effective for the analysis of these ISR data. The aim of the algorithm is to give good stable starting-points for jet-finding. The basic idea is to smear the energy flow with a spatial resolution of the typical size of the structures for which one is searching, i.e. the typical sizes of jets in the kinematic region under consideration. Smaller fluctuations can be removed by appropriate digital filtering, and the surviving structures used as initial values for any convenient method of associating particles into jets. The requisite Fourier mathematics are well-known, and the discrete case is easily adapted to computer analysis.

In the continuous case, for 2-dimensions θ and ϕ, the Fourier transform of the function $E(\theta,\phi)$ is:

$$W(\nu_\theta,\nu_\phi) = \iint E(\theta,\phi)\, \exp[2\pi i(\nu_\theta\theta + \nu_\phi\phi)]\, d\mathrm{Cos}\,\theta d\phi.$$

This can then be filtered by multiplying the transformed function W by a filter function F:

$$W_{filt}(\nu_\theta,\nu_\phi) = F(\nu_\theta,\nu_\phi)W(\nu_\theta,\nu_\phi),$$

where F is a function of the 'frequency' variables ν_θ and ν_ϕ. The filtered transform can then be inverted to give the filtered function:

$$E_{filt}(\theta,\phi) \propto (1/\mathrm{Sin}\,\theta)\iint W_{filt}(\nu_\theta,\nu_\phi)\, \exp[-2\pi i(\nu_\theta\theta + \nu_\phi\phi)]\, d\nu_\theta d\nu_\phi.$$

The filter function $F(\nu_\theta,\nu_\phi)$ is chosen to achieve the desired level of filtering. Donati et al. [11] point out that in principle, for cylindrically symmetric QCD jets, F should be a function of $\sqrt{(\nu_\theta^2+\nu_\phi^2)}$ alone, but that in practice it is more convenient to use a factorizable filter of the form $F(\nu_\theta,\nu_\phi) = F_1(\nu_\theta)F_2(\nu_\phi)$. Filtering of high frequencies removes rapid fluctuations in energy deposition such as those which apparently occur in parton fragmentation, and this is the strength of the method. Filtering of low frequencies could in principle aid in the removal of overall background levels, although this possibility was not deemed necessary for the present analysis.

4.2 Application of the algorithm

In practice the energy of each event is binned in (θ,ϕ) space, using values in the pp c.m., with a cell structure of $N_1 = 30$ bins in θ from 22.5° to 157.5°, and $N_2 = 60$ bins in ϕ from 0° to 360°. These angular ranges approximately cover the c.m. acceptance of our detector. The bin sizes are typical of angular resolutions obtained in the component parts of the detector, and considerably smaller than the typical angular sizes of jets (~30° half-angle) [7] in this $\sqrt{s}$ range. This initial binning of the energy in an event, giving an energy matrix $E(\theta,\phi)$, already smooths the most rapid local fluctuations in energy deposition.

Next the energy matrix is Fourier transformed, using a conventional Fast Fourier Transform algorithm. In the discrete case the transform is:

$$W(\nu_{\theta,j_1},\nu_{\phi,j_2}) = \Sigma\Sigma E(\theta_{i_1},\phi_{i_2}) \exp[2\pi i\{(i_1 j_1)/N_1 + (i_2 j_2)/N_2\}]$$

where the Σ's run over indices $i_1 = 0...N_1-1$, $i_2 = 0...N_2-1$. The physical requirement that the filtered energy flow $E_{filt}(\theta,\phi)$ be purely real (no imaginary component) imposes symmetry requirements on the filter functions F_1 and F_2. The transform must be symmetric around $N_1/2$ and $N_2/2$, i.e. $F_1(\nu_{\theta,j_1}) = F_1(\nu_{\theta,N_1+1-j_1})$ for $j_1 \geq 1$, and similarly for $F_2(\nu_\phi)$.

Following Donati et al. once more, we have chosen to use a filter of the Fermi type, factorizable into independent functions of ϕ and θ, and with parameters chosen so that after filtering the r.m.s. angular size of a delta-function energy deposition becomes that typical of a jet. The explicit functions are:

$$F_1(\nu_{\theta,j_1}) = \{1+\exp[\alpha_1(j_1-1)]\}^{-1}\{1+\exp[\beta_1/j_1]\}^{-1}$$
$$F_2(\nu_{\phi,j_2}) = \{1+\exp[\alpha_2(j_2-1)]\}^{-1}\{1+\exp[\beta_2/j_2]\}^{-1}$$

where $\alpha_1,\beta_1,\alpha_2,\beta_2$ are constants to be chosen, and j_1 runs from 1 to $(N_1/2 + 1)$, and j_2 from 1 to $(N_2/2 + 1)$. The remaining indices are given by applying the symmetry constraint. In these functions, the first term effectively damps high frequencies, and the second damps low frequencies, to a degree depending on the constants α and β. We are insensitive to the precise value of β, since we have not attempted (or found it necessary) to tune the filtering of low frequencies. The value of α, however, determines the degree of "smearing" we are willing to apply to the energy distributions before clustering. The values $\beta_1 = \beta_2 = 3.0$, $\alpha_1 = 0.5$, and $\alpha_2 = 0.25$ were found empirically to smear a delta-function energy deposition in one cell into a structure with a f.w.h.m. angular size of ~15° in both θ and ϕ. Figure 4 shows the variation in this angular width with α_1 and α_2, which are the relevant parameters for this analysis. The width is linear in α_1 and α_2 (separately) over the wide range 0.1 (corresponding to ~ 1 cell in θ or ϕ) to 1.2 (corresponding to ~ 7 cells in θ, 13 cells in ϕ).

The results of the following analysis are stable to considerable variation in the parameters of this filter. This is because the result of the procedure is only to give energy centroids from the surviving energy structures, which are then used as seeds in a trivial iterative procedure in which the original particles detected in the event are associated with the nearest centroid.

The filtered energy distribution is normalized to the total original energy in the event. The filtered energy flow is smoother and more connected than the original flow, and can be clustered simply by merging neighbouring cells containing energy above some low threshold. This threshold is taken as 50 MeV to match the typical minimum detectable energy in the detector elements. The energy centroids of the resulting disjoint clusters are calculated, and the (θ,ϕ) positions of those centroids above a minimum energy E_{min} (discussed below) are used as seeds for building jets.

The jet-finding is completed by using the momentum vectors constructed from each counter hit and charged track in the detector, as discussed previously. Each momentum vector is associated with the nearest centroid, provided that they are within an angular separation of 45°, and once all particles have been tested for association with a centroid the overall jet 4-momenta are calculated from the associated particles. This associative procedure is repeated starting from these jet directions until, in one complete pass through all particles in the event, no particle changes its jet assignment. In general only one or two iterations are required. Some study was made of the sensitivity of the procedure to the minimum number of counter hits (or tracks) required to be associated with a centroid before allowing the cluster to be counted as a "jet". Over 98% of the centroids had at least two hits associated with

them. There were no significant changes in the results if centroids with less than three associated hits were dropped as seeds and the particles allocated to other nearby centroids, if they existed. A centroid with a low associated multiplicity could arise, for example, from a jet which fragments predominantly to neutrals which hit only one shower counter.

The minimum energy, E_{min}, above which an energy cluster is used as a seed for building a jet is chosen to be 2.0 GeV. Approximately 65% of the initial clusters have energies below this, and are discarded, but after association of particles with the surviving centroids, on average over 90% of the total energy in an event is associated with the final jets. As E_{min} is increased the number of jets found tends to decrease, but generally the proportion of the event energy associated with jets also decreases, implying that this does not improve the partition of the energy into fewer jets.

Variation of the limiting angle, within which particles are associated with the energy centroids, from 35° to 55° (normally 45°) leads to only slight variation in the resulting jets. On average, in the final jets, over 95% of the jet energy is contained within a cone of half-angle 30° about the jet direction.

4.3 Event classification

The data were classified according to the number of jets reconstructed by the algorithm. In all events at least one "jet" is reconstructed. Less than 2% of the events have only one jet; approximately 45% have only two jets, 30% have three, and 25% have more than three. In fig. 5a)−c) we show the raw energy-flow in a typical event of each class (2-jet, 3-jet, and more than 3 jets). The height of each tower in the plots represents the energy falling in that cell of θ and ϕ, according to the scale shown. The grid covers the θ range $22.5° - 157.5°$ with 15 cells, and the ϕ range $0° - 360°$ with 30 cells, and hence these cells are considerably coarser than the actual resolution of our detector elements. Corresponding to each event we also show the filtered energy-flow in figs. 5d)−f). These have a reduced vertical energy scale since the energy clusters are now smoothed into continuous distributions. It is clear that the algorithm has successfully identified events which have 2, 3, or more clusters of energy in them.

We denote by E^0_{tot} the total neutral energy measured in an event, calculated in the pp c.m.. Fig. 6 shows the dependence on E^0_{tot} of the numbers of jets reconstructed. The purely 2-jet component gradually rises, the purely 3-jet proportion is virtually constant, and the proportion with more than 3 jets falls. The purely 2-jet and 3-jet contributions quickly become dominant. The overall values quoted

are determined by the proportions just above the trigger threshold, due to the rapidly-decreasing E^0_{tot} spectrum [7].

A more restrictive way of defining the 2-jet sample is to further require that the invariant mass, M, of the two largest jets (calculated from the reconstructed momenta) be greater than some value, while ignoring other jets in the event, if any. We can redefine 3-jet and 4-jet samples analogously. In this way we obtain inclusive jet samples. For example, arbitrarily selecting $M \geq 20$ GeV/c^2, the dependence of the numbers of events on E^0_{tot} is shown in fig. 7. Note that the events in a particular mass-bin come from several bins of the trigger variable E^0_{tot}, and are thus dominated by the lowest compatible E^0_{tot} values.

The number of jets in an event of course depends on the minimum energy a jet is allowed to have. Fig. 8 shows the variation in the numbers of jets per event as a function of this cut-off energy. It is seen that the number of events with more than three jets rapidly decreases to zero as the cut-off is raised.

It is possible that the algorithm be misled by jet-fragmentation fluctuations into spuriously splitting a jet, but this is a small effect according to event displays and the Monte Carlo studies discussed below.

4.4 Correlation with Q values

The Q-Dalitz plots have been examined separately for events reconstructed to 2, 3, or more jets. As expected, the 2-jet events dominantly populate the corner $S \approx 0$, $Q_1 \approx Q_2$, but with tails tending to lie along the upper diagonal. Fewer of the 3-jet events fall in this corner, and they spread further into the body of the allowed triangular region of the Dalitz plot. None of the events with more than 3 jets fall in the corner. In terms of the projections onto the sphericity axis, the 2-jet events have a tightly-constrained S distribution, with a mean value $<S> \approx 0.10$. The S distribution for 3-jet events is broader, with $<S> \approx 0.26$, and that of events with more than 3 jets is very wide, with $<S> \approx 0.48$. A comparison of the three classes is given in Table 1, in which, as well as the mean S values, the proportions of events within certain S ranges are compared.

From these considerations it is found that the events with more than 3-jets populate the allowed region of the Dalitz plot much more uniformly than those with 2 or 3 jets alone. Any event-shape analysis, or even examination of a number of event displays, shows that there are events in which there

are clearly not just two or three tight bunches of energy deposition in the detector. The algorithm will generally reconstruct an isotropic distribution of energy as several "jets" of low and approximately equal energies (c.f. figs. 5c) and f)). This has been verified with Monte Carlo events generated according to phase-space only, and also by analysis of data obtained in 15 GeV colliding α-particle collisions at the ISR, also triggered at 25 GeV total neutral energy in the detector, in which there is little evidence of any jet-like structure. These events populate the Dalitz plot even more uniformly than the more-than-3-jet events in the pp data (although due to the ordering of the Q_i, even perfectly isotropic events will not give a perfectly uniform distribution in the plot). Presumably this implies the existence of bona-fide multijet events within the pp data, which do reconstruct to more than 3-jets.

We are thus led to conclude that in the pp data there appears to be a wide spectrum of events ranging from those in which there are two, three, or even more than three localized energy clusters, to those in which the energy deposition appears to be isotropic.

For completeness, the energy-flow in reconstructed 3-jet events has been plotted relative to the highest-energy jet, in the azimuthal plane defined by the jets in their overall rest frame. As shown in fig. 3d), the recoil jets appear as a significant double-lobe in the flow. The recoil lobes are symmetric because there has been no attempt to orient the second-largest jet in a particular quadrant.

4.5 Angular resolution of the algorithm

The angular resolution of the jet-finding algorithm is measured by mixing well-reconstructed jets from different events, reapplying the algorithm and comparing the reconstructed angular separation with the known true separation. The reconstruction efficiency as a function of the angular separation, for jets of energy above 10 GeV, is shown in fig. 9. The efficiency is zero for separations below about 30° due to the smearing introduced by the filtering, but it rises rapidly to 100% at separations above ~45°. The figure also shows the effect of reducing the filter parameters α_1 and α_2 (described earlier) to half their usual values. A similar study for jets of different energies shows that the efficiency increases from zero less rapidly the lower the jet energy. In all cases full efficiency is attained by a separation of 48°.

4.6 Comparison with Monte Carlo

The classification of events into two, three or more jets is not unambiguous even in principle. The number of jets seen in the final state depends to some extent on the resolution with which the state is

examined, and the definition of what a "jet" is taken to be. To demonstrate the typical difficulties involved Monte Carlo (M.C.) data generated with the ISAJET 4.0 program [12] were analyzed with the same algorithm. This version of ISAJET did not model initial-state bremsstrahlung and so was not expected to predict as many 3-jet events as seen in the data. ISAJET generates a final state of two partons, each of which can evolve into several partons of lower energy, which are then fragmented into hadrons. Each of these evolved ("final-state") partons, which we abbreviate as "f.p.", corresponds to a final-state "jet". A cutoff energy is chosen at which this cascading terminates and fragmentation begins. The relative number of 3-jet and 2-jet events (3 or 2 f.p. respectively) depends on the input value of α_s, but the resulting events show properties (e.g. jet angular distributions) reflecting the leading-log approximation to the QCD cross-sections used in the program. The geometrical acceptance of our detector was applied to the generated events, but no attempt was made to model the E^0_{tot} trigger which is sensitive to only a few percent of the jet cross-section, and would therefore require an enormous increase in computer time. Thus we could only use the M.C. to study properties which did not depend on the particular jet fragmentation. For example, it is to be expected that the ratio of charged to neutral energy in the jets be different in the data and in the M.C.. In order to obtain any pairs of jets with angular separations less than about 60° it was found necessary to reduce the cutoff energy from the nominal value of 7 GeV to 3 GeV. The question of the physical validity of making this change is irrelevant, since we have only used the M.C. to study the resolution of the jet-finding algorithm. The algorithm gives quite stable results without further adjustment of its parameters. It is found that, as expected, there is a broad intermixing of events with 2 or 3 f.p. when reconstructed to 2-jet and 3-jet events. About 60% of the reconstructed 3-jet events have 3 f.p., and about 80% of the 2-jet component have 2 f.p.. The dominant contamination of the reconstructed 2-jet sample is due to the merging of two jets in events with 3 f.p.. That of the 3-jet sample is predominantly due to the spurious splitting of one jet in a small fraction (~1.5%) of the events with 2 f.p.. Since this version of ISAJET predicts a 3-jet/2-jet (i.e. 3 f.p./2 f.p.) ratio of about 10% (and with no provision for initial-state gluon bremsstrahlung), even a small misidentification of 2-f.p. events can cause a large contamination of the 3-jet sample. By examining the fraction of 3-f.p. events found in the 3-jet sample we have measured the angular separation, α_{23}, between the two jets with lowest energies, and compared it to the angular separation between the original parton directions. The correlation is shown in fig. 10. There is a slight systematic shift between the the two values, so that the measured angles tend to be higher than the real

values for angles below about 45°. Nevertheless the mean values of the angular separations between the reconstructed jet axes agree closely with the corresponding parton values, so that the directions of the reconstructed jets reproduce those of the underlying partons.

Less than 1% of the ISAJET events are reconstructed to more than 3 jets, hence substantiating the claim that this class is not filled by spuriously-split 2- or 3-jet events.

From these ISAJET studies we can conclude that:

1. The reconstruction algorithm is well-behaved, and succeeds in identifying those events with 2 or 3 final-state jets;

2. The reconstructed jet directions match the parent parton directions quite closely; and

3. There are virtually no events with more than 3 jets in the Monte Carlo data, thus showing that such events in the real data do not arise by spurious splitting of 2-jet or 3-jet events.

5. Event properties

The properties of the 2-jet events reproduce those presented with the more conventional method of 2-jet analysis in ref. 7 (which used a subset of the data analysed in this paper), including energy spectra, angular separations of the jet axes, and fragmentation properties of the jets. In this section we discuss general properties of the jets, and leave the fragmentation j_T and charge ratios within the jets until the next section.

The jets within each event are ordered by decreasing energy, so that jet 1 is the jet of highest energy. Table 2 shows the mean energies of the jets in each event class, and Table 3 the corresponding mean transverse energies. The mean ratio of transverse to total energy in the jets is almost independent of event class, with a value ~ 0.85. The energy spectrum of the lowest-energy jet, jet 3, in events with exactly three jets is shown in fig. 11. It is seen that this energy spectrum does not fall sharply from the E_{min} value of 2.0 used, but peaks at about 5.5 GeV. Presumably, the fall-off below the peak is an artefact of the reconstruction. The mean fractional neutral energy in each jet, $<E^0_{jet}/E_{jet}>$, is about 0.75. Such a value is in fact also typical of π^0-dominated jets obtained by triggering on a single high p_T neutral cluster at the ISR [13].

As in ref. 7, the two jets in 2-jet events tend to be 180° apart in azimuthal angle. In the 3-jet events, the two largest jets also tend to be 180° apart, although with a much broader distribution. The r.m.s. widths of these distributions are given in Table 4. The distribution of the angular separation between the two smaller jets, α_{23}, in 3-jet events is shown in fig. 12. This shows that jets 2 and 3 tend to be close to each other, and hence recoil together against jet 1. This is true of the ISAJET M.C. 3-jet events too. Also shown in fig. 12 is a phase-space distribution (actually obtained from randomizing the particles in real events according to the prescription discussed in the "Jet fragmentation" section). The mean values of the α_{12} and α_{23} distributions are listed in Table 4 for each event class.

6. Jet fragmentation properties

6.1 Introduction

A characteristic property of a jet is that the particles comprising the jet have a limited transverse momentum, j_T, relative to the jet axis. This is apparently a general feature of the fragmentation process. This fragmentation j_T has been studied previously for 2-jet events in ref. 7. The charge ratios of the leading charged particles in the jets may yield information about the charge of the fragmenting parton. These properties are examined in the following sections.

6.2 Jet sample definition

We follow the notation of ref. 7, and likewise restrict our analysis to the charged particles within each jet, since the separation of individual particles is clear, and the angular resolution is better than that for neutrals. The mean number of charged particles (with momentum > 300 MeV/c) per jet is about two (in all event classes), although ~15% of the jets contain purely neutral energy.

For clarity and simplicity, in these fragmentation studies we have used just those events with exactly two or exactly three jets. Furthermore, in order to avoid any possible effects of the E_{min} value of 2 GeV used in the reconstruction, events with jets of energy below 4 GeV (< 10% of the events with exactly three jets) were not used. The fragmentation properties are found to be insensitive to cuts on the energy in the events and to the proportion of event energy in the jets. We have required $\Sigma E^{Q}_{jet} \geq 20$ GeV for both event classes. No significant change, except in event statistics, is seen if this

cut is varied. ISAJET studies confirm the expectation that in a 3-jet event the jet energy tags the probability that the parent parton was a quark or gluon, i.e. the lowest-energy jet is more likely to arise from a gluon: a jet in a 2-jet event has a ~60% probability to be from a u-quark, and the lowest-energy jet in a 3-jet event has a probability of ~75% to be from a gluon.

To minimize possible acceptance effects at the edges of the detector, we impose the requirement that a cone of certain half-angle about each jet axis be fully-contained within the e.m. acceptance. This requirement also minimizes acceptance differences between the jets of 2-jet and 3-jet events. Since it is known that the core of a jet is most important [7], and to maximize statistics, a half-angle of 10° is used. Variation of this angle from 5° to 25° has no effect on the charge-ratio results, within the statistical errors.

6.3 The fragmentation transverse momentum

Over the full jet-energy range (8 to 28 GeV), the j_T values obtained for the 2-jet events reproduce those presented in ref. 7, showing that the 2-jet events are not biased by the new reconstruction procedure.

Figure 13a) shows the behaviour of the mean j_T of the charged particles in the lowest-energy jet in 3-jet events as a function of z, the fragmentation variable defined by $z = p_\parallel / E_{jet}$, where $p_\parallel$ is the longitudinal component of the particle momentum along the jet direction, and E_{jet} is the jet energy. Use of z approximately scales out the jet energy so that the jet-energy bins many be combined in studies of the dependence of fragmentation properties on $p_\parallel$. Since only tracks with momenta above 300 MeV/c have been reconstructed, values of z below 0.075 are suppressed. The E_{jet} range is restricted to the $4-8$ GeV range in which most of the jet 3 data lie. The j_T plateau in this plot shows the characteristic 'seagull' behaviour due to limited transverse momentum in the jet fragmentation process. Also shown in the figure is a curve obtained from random events. These are generated from real events [7]: The azimuthal angle, ϕ, and the rapidity, y, of each charged-particle momentum vector in an event are randomized (but subject to the constraints that the overall ϕ and y distributions remain the same as for the original events) and the events are reanalyzed into jets. The α_{23} distribution from such events, but randomizing all momenta, has already been displayed in fig. 12. Only those randomized events leading to three "jets" (clusters of particles) are used, so that the algorithm selects those random events in which there is some clustering of "jet-3" particles. This reduces the random j_T from the linear in-

crease with z which might have been expected (as seen e.g. in ref. 7). There is little difference in the results obtained from analysis of three sets of randomized events: a) those obtained by randomizing all momenta of particles in the full event sample, b) those from randomizing just the real 3-jet events, or c) those from randomizing just the charged particles in the real events. The j_T for these randomized data also tend towards a plateau as z increases, but at a significantly higher level than the real data. This shows that the limited nature of j_T in the real events is not just a kinematic constraint of the detector acceptance.

Since the expectation is that the lowest-energy jet in the 3-jet events is more likely to be from a gluon than a quark, it is useful to compare jet 3 with a sample of jets which are more likely to be from quarks. Although we might hope that use of the variable z has already scaled out any E_{jet} dependence, it is clearly better to use jets in the same energy range for this comparison. In the 2-jet sample there are few events with a jet of such low energy as the jet 3's in the 3-jet sample, and those that are so low are associated with particularly high energy jet 1's so that the two jets are particularly asymmetric. Thus a sample of low energy jets in 2-jet events was obtained by analysis of data collected in pp collisions at $\sqrt{s}$ = 52 GeV, with a trigger requiring two back-to-back depositions of neutral energy in our detector, each cluster being over 3 GeV. These triggers are mainly 2-jet events, in which each parton fragments predominantly to π^0's, and in this kinematic region, since $x_T = 2p_T/\sqrt{s}$ is relatively high, a large proportion of these partons should be quarks. Figure 13b) compares the mean charged j_T measured for the lowest-energy jet in 3-jet events with that of jets in 2-jet events from the $\pi^0\pi^0$ trigger data, both restricted to the E_{jet} range $4-8$ GeV. The two sets of values appear to be perfectly consistent with each other. However, we expect that the third jet in 3-jet events has less available phase space than the jets in 2-jet events, due to the presence of the other jets. We have attempted to correct for this reduced geometrical acceptance by comparing the values for j_T obtained from fake 2-jet and fake 3-jet events, whilst ensuring that the jet energies are sufficiently close that j_T differences cannot be due to energy differences. The results are displayed in fig. 13c), where it is seen that the fake 2-jet values are indeed larger than the fake 3-jet values, in each z-bin. The ratio of these values, also plotted in the figure, is virtually independent of z, with a value of about 0.8. We believe that systematic effects are sufficiently small that this difference is significant. Thus a first-order correction to the j_T measured for jet 3 in real 3-jet events is just to increase it by a factor of $1/0.8 = 1.25$.

We thus conclude that that the constrained nature of the j_T in the jets confirms that we are dealing with bona-fide "jets", even for the lowest-energy jet in 3-jet events. The magnitude of the uncorrected j_T is approximately the same for jet 3 in 3-jet events and for jets of the same energy in 2-jet events, although a first-order acceptance correction for the reduced acceptance available to jet 3 in 3-jet events leads to values of j_T for jet 3 which are about 25% larger than the 2-jet values at similar jet energies.

6.4 Charge ratios in the jets

The ratio of the number of positive to the number of negative charged particles in a jet is expected to be related to the charge of the parton which fragments into the jet. Likewise, the charge of the parent parton should be reflected in the charge of the leading charged particle in the jet, where this is the charged particle of highest z. This ratio should not be sensitive to our trigger requirement which, on the other hand, presumably lowers the total charged/neutral energy fractions within the jets from their untriggered values. The leader charge-ratio asymmetry

$$R = [N^+ - N^-]/[N^+ + N^-]$$

is defined where N^+,N^- are the numbers of jets with leading charged particle positive or negative respectively. This ratio is shown as a function of the z of the charged particle in fig. 14a), for jet 3 in 3-jet events, and for both jets in 2-jet events, integrated over the most populous jet-energy bins (4 − 8 GeV for 3-jet, 8 − 28 GeV for 2-jet). Figure 14b) shows the same charge ratio from jet 3 in 3-jet events, but now with the ratio measured in the 2-jet $\pi^0\pi^0$ events, so that both jet-energy ranges are 4 − 8 GeV. The solid curve represents the ISAJET prediction for the values expected from a mixture of two-thirds u-quark and one-third d-quark jets. The expected value from gluon jets is zero. It is clear that whereas the 2-jet ratio is positive and significantly different from unity, and appears very well-described by the predicted value for a 2:1 mixture of fragmenting u- and d-quarks, the 3-jet value is consistent with zero, as expected for the fragmentation of a neutral parton (gluon). Since the initial state of two protons has a charge of + 2, an enhanced positive asymmetry could be a trivial result of charge conservation, although this is not expected since our detector is not sensitive to particles of large rapidity at small transverse momentum. That this is indeed not the case has been shown in ref. 7, where it was demonstrated that only in the core of a jet (< 30° from the jet axis) does the charge ratio

show a significant positive excess, which increases closer to the jet direction. It should be noted that in the 2-jet events the jet energies are higher than those of the lowest-energy jets in 3-jet events, and this could influence the value of the charge ratios since the dominant parton type is expected to change with the jet energy, reflecting the Bjorken x distributions of the partons (structure functions) within the colliding protons.

We have presented a detailed discussion of the effect of possible systematic error on the charge ratio in ref. 7. This discussion is directly relevant since the data in that reference are a subsample of the present set. There we concluded that systematic errors were not significantly distorting the charge ratios; we believe that this conclusion is still applicable.

In summary, the leading charged particles are dominantly positive in the jets from 2-jet events, as expected for dominant u-quark fragmentation. However there is no charge asymmetry in the charged leaders from the lowest-energy jet from 3-jet events. This too is expected if gluons are the dominant fragmenting partons in this case.

7. Estimation of an effective α_S

7.1 Introduction

We have estimated an effective "α_S" value from the relative numbers of 2-jet and 3-jet events in our data. After triggering on large transverse energies (our detector is centred at 90°) we expect to detect events in which there is a large subprocess momentum-transfer. Guided by Quantum Chromodynamics (QCD), we naively expect 3-jet and 2-jet events to occur in the ratio of α_S, assuming that we are measuring events at the same subprocess momentum-transfer squared (Q^2). We have only reconstructed jets in the final state, so that the estimation of Q^2 is non-trivial. In practice we shall work in terms of the invariant mass of the final jet system; this mass is an estimate of the $\sqrt{s}$ of the parton subprocess, $\sqrt{\hat{s}}$. For our data, this is about 25 GeV/c^2.

We emphasize that we have not attempted to correct for two possible distortions of the observed 3-jet/2-jet ratio from the actual one which are difficult to unfold from the data. First, the measured jet energies have not been corrected to account for undetected particles (e.g. K_L, n, ν). Second, the E^0_{tot} trigger might distort the ratio. Nevertheless, in view of the interest in α_S estimates obtained from ha-

dronic interactions, and because our 3-jet and 2-jet events were collected in the same apparatus with the same calorimetric trigger, we feel that it is worthwhile to proceed with an analysis ignoring these effects.

7.2 Method

We follow the straightforward approach of integrating the leading-order (l.o.) QCD cross-sections over regions corresponding to our detector acceptance and over 3-jet angular configurations that we can resolve, and hence estimate α_S by comparison with the measured ratio of 3-jet/2-jet events. This approach has previously been taken by the UA1 collaboration [4] at the higher $\sqrt{s}$ values available at the SPS Collider. The l.o. QCD cross-sections for $2 \to 2$ and $2 \to 3$ parton subprocesses are now well-known [14,15,16,17]. The 2-jet cross-section can be written as:

$$\sigma_2 = \frac{\pi}{2} \frac{\alpha_S^2}{\hat{s}} |\mathcal{M}_{2\to 2}|^2$$

and the 3-jet one as:

$$\sigma_3 = \frac{1}{16\pi} \frac{\alpha_S^3}{\hat{s}} |\mathcal{M}_{2\to 3}|^2$$

where $|\mathcal{M}|^2$ are the squared-matrix elements for the individual $2 \to 2$ or $2 \to 3$ processes. A typical result for $|\mathcal{M}|^2$ from ref. 14 is that for a $2 \to 3$ quark-quark scattering with different flavours,

$$q_1(p^+) + q_2(p^-) \to q_1(q^+) + q_2(q^-) + g(k).$$

The result is:

$$\begin{aligned} |\mathcal{M}|^2 = {} & (1/8)G^6[(s^2+s'^2+u^2+u'^2)/tt'][(p^+k)(p^-k)(q^+k)(q^-k)]^{-1} \\ & \times \{A_1[(u+u')(ss'+tt'-uu')+u(st+s't')+u'(st'+s't)] \\ & - A_2[(s+s')(ss'-tt'-uu')+2tt'(u+u')+2uu'(t+t')]\}, \end{aligned}$$

after averaging over colour degrees of freedom for the initial states, and summing over those for the final states. In this, and the equivalent expressions for other parton combinations, G is the SU(N) gauge coupling constant (we take $N=3$, for 3 colours), and $A_1 = (N^2-1)^2/4N^3$, $A_2 = (N^2-1)/4N^3$. The 4-momentum invariants s,t,u,... are conventionally defined:

$$s=(p^+ + p^-)^2,\ t=(p^+ - q^+)^2,\ u=(p^+ - q^-)^2,$$

$$s'=(q^+ + q^-)^2,\ t'=(p^- - q^-)^2,\ u'=(p^- - q^+)^2.$$

The $|\mathcal{M}|^2$ can be expressed in terms of variables measured in the final 2-jet or 3-jet rest-frame. In the 2-jet case, only one variable is required, and this is taken as θ, the parton scattering angle. In the 3-jet case the jets are ordered by $x_i = 2E_i/\Sigma E_i$ where E_i is E_{jet} for jet i, so that $x_1 \geq x_2 \geq x_3$. Then $x_1 + x_2 + x_3 = 2$ and all $x_i \leq 1$. Again we follow the conventional choice, and take the four variables x_1, x_2, Cos θ_1, and ψ, where Cos θ_1 is the angle between jet 1 and the parton collision axis, and ψ is the angle between the plane containing the three jets and the plane defined by the colliding partons and jet 1 (see fig. 15). The angle θ_1 ranges from 0 to 180°, and ψ ranges from 0 to 360°. We define coefficients C_2 and C_3 by:

$$\sigma_2 = C_2\alpha_S^2/\hat{s}, \quad \sigma_3 = C_3\alpha_S^3/\hat{s}$$

where C_2 and C_3 are the integrated partonic cross-sections (including constant factors) for specific $2 \rightarrow 2$ and $2 \rightarrow 3$ processes respectively. Assuming that the 2-jet and 3-jet events can be compared at the same effective Q^2, so that two powers of $\alpha_S(Q^2)$ cancel, we see that:

$$\sigma_3/\sigma_2 = \alpha_S,$$

or, more precisely,

$$\sigma_3/\sigma_2 = \alpha_S(K_3/K_2)$$

where the K factors account for higher-order corrections to the l.o. QCD expressions.

To obtain the theoretical ratio of the cross-sections we use the full l.o. QCD expressions for $2 \rightarrow 3$ processes given by Berends et al. [14], supplemented by Halzen and Hoyer [17]. A typical example, for $qq \rightarrow qqg$, has been given explicitly above. We have checked analytically and numerically that these expressions reduce to the 90° c.m.s. cross-sections given in ref. 15. Note that in evaluating the integrals of the cross-sections we must add contributions for all distinguishable permutations of the final-state partons. The 3-jet/2-jet comparison must of course be restricted to regions of phase space in which all the jets are well-separated from each other and from the beams. The l.o. 3-jet cross-sections diverge for configurations which approach 2-jet ones (i.e. x_1, $x_2 \rightarrow 1$) due to initial/final-state gluon bremsstrahlung. We numerically integrate the full expressions over several different regions of the variables, corresponding to different ranges within our acceptance. The widest range used is still well-contained within the uniform acceptance region of our detector. We have also checked that we reproduce the values obtained by UA1 for their particular choice of cuts [4]. Our results for three typical sets of cuts are given in Tables 5, 6 and 7; these cuts will be discussed in greater detail below. The theoretical calculations have been made for the elastic $2 \rightarrow 2$ and single gluon $2 \rightarrow 3$ processes only, with

initial states gg, qg, qq, and qq′. The identical flavor qq and different flavor qq′ processes give slightly different values, and we have assumed a 50% equal contribution of each, although changing the proportion hardly affects the results. Antiquark contributions are negligibly small for our kinematic regime. It is found that the integrated theoretical ratios are not strongly dependent on the subprocess, which means that we are not strongly sensitive to the precise proportions of the subprocesses contributing to the data.

7.3 Choice of structure functions

Although we find that the dependence of the integrated theoretical cross-sections on the exact parton subprocess is small, we have in fact estimated these proportions using the Lund Monte Carlo PYTHIA [18] for 2-jet events (each of energy about 15 GeV) in pp interactions at $\sqrt{s}$ = 62 GeV. This uses the EHLQ [19] structure functions resulting in 64% qq : 34% qg : 2% gg. They have also been estimated by the AFS collaboration [8] for rather similar conditions as the present experiment as 54% qq : 40% qg : 6% gg using Duke-Owens [20] structure functions, but which the authors argue should be modified to 70% qq : 28% qg : 2% gg, due to the softness of the gluon structure function which they themselves have measured. We then compare our measured ratio of 3-jet/2-jet events to a weighted sum of the events predicted assuming these proportions [64%:34%:2%]. We also assume an equal contribution from qq and qq′ processes. The sensitivity of the extracted value of α_s to these proportions will be discussed below. Thus explicitly, we calculate $<C_3/C_2>$ as $(a_1C_{31} + a_2C_{32} + a_3C_{33})/(a_1C_{21} + a_2C_{22} + a_3C_{23})$ where a_j is the fraction of subprocess j (qq, qg, or gg) and C_{ij} is the corresponding coefficient C_i from the tables.

Assuming massless partons, with no initial p_T, the Bjorken x's of the colliding partons can be calculated from the momenta of the final jets. For our data the mean x values of the faster and slower incoming partons are 0.53 and 0.32 in 2-jet events, and 0.54 and 0.34 in 3-jet events.

7.4 Event selection

For the α_s analysis the events are processed by the jet-finding algorithm as usual except that we neglect charged particles which do not fall (at production) within the acceptance of our e.m. calorimeter. This minimizes the acceptance difference between the reconstructed 2-jet and 3-jet events, and hence simplifies the comparison. On average this means neglecting one or two charged particles per event, containing about 1.1 GeV of energy − equivalent to about 3% of the total energy in the event.

The 2-jet sample is composed of all events with at least 2 reconstructed jets, in which any other than the 2 largest-energy jets are ignored. The 3-jet sample is defined analogously. If we simply calculate the invariant mass of the jets in the 2-jet and 3-jet samples, and plot the ratio of 3-jet/2-jet against the mass, we obtain fig. 16. There is a rise from low masses, reaching a plateau for masses above about 20 GeV/c^2. The value of the plateau is not expected to be directly related to the value of α_s because of various acceptance and efficiency differences (in both detection and reconstruction) between the event samples. The cause of the decrease in the ratio at lower masses is two-fold. First, the "isotropic" events in which we have taken two or three "jets" containing relatively small proportions of the event energy populate this region. Second, there is a relation between the invariant mass and the total energy of a 3-jet system. At fixed total energy of the jets, each angular configuration corresponds to a different mass, and vice-versa. This means that low-mass 3-jet events tend to have a pair of close jets, which are not resolved by the algorithm so that the 2-jet class is enhanced.

We then require that the neutral energy in the jets under consideration, ΣE^0_{jet}, be above 22 GeV (c.f. section 7.6) to ensure that the trigger was fully efficient, and satisfied by the neutral energy in the jets alone. Since the jet classes may overlap, the 2-jet and 3-jet samples are inclusive. The jets are transformed into the rest-frame of the multijet system. The mean jet energies in the multijet rest-frame are shown in Table 8. The distribution of the overall p_T of the events has a peak at ~ 4 GeV/c and a tail extending to ~ 20 GeV/c. The mean p_T is found to be independent of the jet class, and decreases slowly with ΣE^0_{jet} from ~ 5 to ~ 4 GeV/c. We have chosen to require $p_T < 13$ GeV/c in order that only the most well-balanced, and hence presumably well-measured, events are used for the evaluation. The variables x_1, Cos θ_1, and for 3-jet events also x_2 and ψ, are calculated. Since the colliding partons may have different fractions of the colliding proton momenta (i.e. their Bjorken x's are in general unequal), they are not in general collinear in the final multijet rest frame. The conventional Collins-Soper choice [21] is used: θ is measured as the polar angle between jet 1 and the direction making equal angles with the two transformed beam directions,. and hence has a range from 0 to 90°. The angle ψ is measured in a similar way, and has a range 0° to 180°. For the 3-jet events the x_i are recalculated from the jet angles, since this improves the x_i resolution, and perhaps compensates to some extent for misassignment of energy amongst the jets. This is done by inverting the three relations:

$$\text{Cos } \alpha_{jk} = 1 - 2[(x_j + x_k - 1)/x_j x_k]$$

where α_{jk} is the angle between jets j and k.

7.5 Detector acceptance

The variables Cos θ_1 and y_{mj} (where y_{mj} is the rapidity of the multijet system in the pp c.m.) should be independent, so that any non-uniformity in the distributions of events in the (Cos θ_1, y_{mj}) plane is due to a coupling resulting from the acceptance of the detector. It is found that both the 2-jet and 3-jet events are uniformly distributed within well-defined regions in this plane. In these regions the detector acceptance is uniform, and from the distributions the limits of acceptance in Cos θ_1 can be extracted. These are about ± 0.6 for 2-jet events and ± 0.4 for 3-jet events (although the distributions in Cos θ_1 extend to ± 0.7 and ± 0.6 respectively). Likewise the limits in y_{mj} are about ± 0.4. We have estimated α_s using several sets of cuts, each contained within this region of uniform acceptance. In each case we restrict $|y_{mj}| \leq 0.4$. Each set of cuts is labelled by four values: one for the 2-jet events [max |Cos θ|], and three for the 3-jet events [max |Cos θ_1|, min ψ, max x_1]. The results of the integration of the theoretical cross-sections over three of these sets, including the the widest and narrowest of these ranges, are given in Tables 5, 6 and 7. The loosest set is defined by 2-jet |Cos θ| $\leq$ 0.6, with 3-jet $x_1 \leq 0.92$, |Cos θ_1| $\leq$ 0.4, $45° < \psi < 135°$, and the tightest set is defined by 2-jet |Cos θ| $\leq$ 0.3, with 3-jet $x_1 \leq 0.9$, |Cos θ_1| $\leq$ 0.2, $60° < \psi < 120°$.

7.6 Agreement with QCD

A typical jet-energy Dalitz plot for 3-jet events, given as is now usual as a plot of x_2 against x_1, together with the x_1 and x_2 projections, is shown in fig. 17 for the set of cuts of Table 6. The events are selected rather loosely with multijet invariant masses $M \geq 20$ GeV/c^2 and $\Sigma E^0_{jet} \geq 19$ GeV; the general features of the plot are unchanged with more stringent cuts. The solid curves are l.o. QCD predictions, normalized to the same total number of events as the data. The QCD predictions for the four dominant subprocesses are very similar. Here we show an admixture weighted by the structure functions predicted by the Lund Monte Carlo as discussed in section 7.3: 64% qq + 36% qg. The dashed lines show the expectation from phase space alone (i.e. constant matrix element). In these plots the density of events increases both with x_1 and with x_2, as expected from the QCD bremsstrahlung process, and the x_1 and x_2 projections seem to be well-described by the QCD predictions. The distribution in x_1 in fact continues rising until there is a sharp turnover and rapid decrease to zero for x_1 above ~ 0.96. This turnover is due to the inefficiency of the jet-finding algorithm as two of the jets merge. There is a direct correlation between increasing x_1 and decreasing angular separation between

functions, 10% from uncertainty in the acceptance correction, 15% from systematic variation with mass and ΣE^{Q}_{jet} cuts, and 8% from variation of the inclusive sample definition. This yields an estimate of the possible systematic error of 21% in $\Delta\alpha_S/\alpha_S$, equivalent to ± 0.039 in α_S itself. Note that most of these corrections tend to *increase* the value of α_S.

7.10 Final value and choice of Q^2

Our measured value for α_S is

$$\alpha_S(K_3/K_2) = 0.19 \pm 0.02 \text{ (stat.)} \pm 0.04 \text{ (syst.)}.$$

The choice of Q^2 at which to evaluate the QCD cross-sections is an open and difficult question. The UA1 collaboration has some indications [22] that the choice $-\hat{t}$ is preferred by their 2-jet data, and that the choice $\hat{s}$ is in fact ruled out. The choice $-\hat{t}$ was used in QCD-inspired studies of the parton scattering angle distributions in ref. 13. In our data the value of $\hat{t}$ can be calculated for the 2-jet events, and the mean value $<-\hat{t}>$ correlates well with the mean p_T^2 of the events, with $<-\hat{t}> \approx 1.75 <p_T^2>$. The range of $-\hat{t}$ covered is from about 200 to 400 $(GeV/c)^2$, with a mean value of 323 $(GeV/c)^2$, much lower than the values ~ 4000 $(GeV/c)^2$ typical of the SPS Collider data. For want of evidence to contrary, and since our available $\hat{t}$ range is extremely constrained in comparison with that explored at the Collider, we assume that the same Q^2 is relevant for both the 3-jet and 2-jet events we have measured and compared. If we follow UA1, and scale Q^2 by M (the invariant mass of the jet system), for the 2-jet sample we find $<\sqrt{Q^2}/M> = 0.57$, and a similar value for the 3-jet sample, $<\sqrt{Q^2}/M> = 0.60$. Thus our measured value is:

$$\alpha_S(K_3/K_2) = 0.19 \pm 0.02 \text{ (stat.)} \pm 0.04 \text{ (syst.)}$$

at $Q^2 = -\hat{t} \approx 300$ $(GeV/c)^2$. This value appears to be in remarkably good agreement with those already obtained from hadronic collisions at the ISR and SPS [4,5,8].

The expected dependence of α_S on Q^2, according to standard renormalization group considerations, is:

$$\alpha_S(Q^2) = 12\pi/[(33-2n_f)\ln(Q^2/\Lambda^2)]$$

where $\Lambda = \Lambda_{QCD} = 0.2$, and n_f is the number of flavours. Taking $n_f = 4$ we thus expect $\alpha_S(Q^2 = 300) = 0.17$, and to vary from about 0.18 to 0.16 over our Q^2 range. We are insensitive to a variation of this magnitude.

- The variation in the extracted $\alpha_S(K_3/K_2)$ obtained by using the three different sets of subprocess fractions discussed earlier is small: changing from the EHLQ fractions to the Duke-Owens fractions for the cuts in Table 6 changes $<C_3/C_2>$ from 0.453 to 0.483. This changes $\alpha_S(K_3/K_2)$ from 0.185 to 0.174, a shift comparable to only half the statistical error, but nevertheless we assume a contribution to the systematic error of $\Delta\alpha_S/\alpha_S = 5\%$.
- A clear possible source of systematic error lies in the value of the weight accounting for the relative 3-jet to 2-jet acceptance. The weight shows a dependence on the cone-angle used to characterize the jet acceptance. This mean value increases from about 1.3 to 1.5 as the cone angle is increased from 5° to 20°. In fact the value of the weight tends to compensate for acceptance losses due to the cone size. For example, for the cuts of Table 6, the mean weight is 1.39 for a 10° cone, and 1.34 for a 5° cone, but the corrected ratios of 3-jet/2-jet are identical. We follow the conservative approach of estimating the possible systematic error in $\alpha_S(K_3/K_2)$, due to systematic error in this weight, by taking extreme limits in the value of the weight and repeating the calculations. These limits are taken as 1.25 (i.e. considerably underweighting the measured number of 3-jet events) and 1.45 (i.e. considerably overweighted). For the cuts of Table 6 the resulting shifts in $\alpha_S(K_3/K_2)$, from the original value 0.185, are to 0.166 and 0.193 respectively. Accordingly we add a contribution to the systematic error of $\Delta\alpha_S/\alpha_S = 10\%$.
- To account for possible residual systematics in the event selection, we have examined the variation in the ratio of 3-jet/2-jet as the cut on the neutral energy in the jets, ΣE^0_{jet}, is varied from 20 to 25 GeV, and the cut on the invariant mass of the jets, M, is correspondingly increased such that $M \geq \Sigma E^0_{jet} + 5$ GeV. The variations in $\Delta\alpha_S/\alpha_S$ are within $\pm 15\%$. We assign a generous contribution to the systematic error of 15%.
- To investigate whether the inclusive criterion for the 2-jet and 3-jet jet sample could distort the value of the ratio, we have repeated the analysis but restricting the events to be those with two and only two jets in the 2-jet sample, and three and only three jets in the 3-jet sample. The result is to reduce α_S by $\Delta\alpha_S/\alpha_S = 8\%$. Again we allow a generous contribution to the possible systematic error of 8%.

Consequently the overall estimate of systematic error is made by adding the various above contributions in quadrature: 6% from the spread with different cuts, 5% due to uncertainty in the structure

events by the corresponding number of 2-jet events. The values in the column headed '$< C_3/C_2 >$' are evaluated from the numbers corresponding to those in Tables 5−7 (for the appropriate cuts), using the relative proportions of qq, qg, and gg subprocesses predicted by the Lund M.C., also as discussed earlier. Finally, the estimates of $\alpha_S(K_3/K_2)$ shown in Table 9 are obtained from the ratios $(\sigma_3/\sigma_2)/< C_3/C_2 >$. The errors quoted in this table are purely statistical. It is evident that the values obtained from each set of cuts are consistent (although they are not statistically independent).

7.9 Stability of results and estimate of systematic error

Since the evaluation has been made by forming a ratio of numbers of 3-jet and 2-jet events collected in the same apparatus at the same time, many systematic errors cancel out, or are at least minimized. In particular the error on the integrated luminosity does not contribute to the error on $\alpha_S(K_3/K_2)$. We estimate the systematic error on the final value of α_S after studies of the variation of the value with the several points. These are listed below, together with the corresponding contribution to the error, where appropriate:

- The analysis performed for the sets of cuts in Table 9 was followed for many combinations of the cuts in variables (2-jet Cos θ in the range 0.6 to 0.3, 3-jet Cos θ_1 in the range 0.4 to 0.2, and ψ in the range $45°-135°$ to $60°-120°$). The spread of values obtained is from 0.17 to 0.19, just as seen in the subset presented in Table 9; we thus assign a contribution to the final systematic error of $\Delta\alpha_S/\alpha_S = 0.01/0.18 = 6\%$.
- The seed value , E_{min}, could affect the number of 3-jet events reconstructed, although the upper limit on x_1 corresponds to a lower limit on x_2, and hence is equivalent to a cut on the energy of the lowest-energy jet. Using E_{min} values of 1 or 3 GeV, instead of the usual 2 GeV, changes σ_3/σ_2 by an amount less than one-third of the statistical error for all sets in Table 9. No contribution to the systematic error is taken.
- Reducing the filter parameters α_1 and α_2 to half their standard values changes σ_3/σ_2 by less than one-half of the statistical error. No contribution to systematic error.
- Changing the relative proportions of qq and qq′ from equal to entirely qq (no qq′) has a negligible effect on the averaged ratio $< C_3/C_2 >$; for example, for the cuts in Table 6 the value remains 0.453. No contribution to systematic error.

jets 2 and 3: Cos $\alpha_{23} \leq 4-3/x_1$. We choose events with $x_1 \leq 0.92$, which corresponds to requiring the angle between jets 2 and 3 (the closest pair of jets) to be at least 42°, where the algorithm is fully efficient as shown earlier. An analogous plot can be made for Cos θ_1 against ψ (c.f. ref. 4), and again the projections show better agreement with QCD than with phase space, but the ranges of these variables (particularly in Cos θ) are restricted quite severely by the requirement that our detector acceptance be uniform there, and the statistical significance is low. The consistency with QCD is apparent, however, in the 2-jet angular distribution. A typical Cos θ distribution for the jet axis in 2-jet events is shown in fig. 18. Only the absolute value of Cos θ is determined, and both the real distribution and the overlaid QCD prediction have been normalized to 1.0 at $|\text{Cos}\ \theta| = 0$.

After restricting the events to lie within the reduced angular regions (c.f. section 7.5), and with the x_1 cut, and cuts on the overall p_T and y_{mj}, we can again examine the dependence of the ratio 3-jet/2-jet on the invariant mass of the jets. We find that this ratio is constant once we restrict ourselves to masses above ~28 GeV/c^2, and ΣE^q_{jet} above ~22 GeV. These cuts are applied to the data.

7.7 Acceptance corrections

Finally, the observed number of 3-jet events must be corrected for acceptance effects. Since it is only the relative 3-jet to 2-jet acceptance which is important, the only correction necessary is for the limited acceptance available for three jets relative to two jets in the detector. This correction was made following the UA2 procedure [5]. A weight is associated with each 3-jet event to account for the limited ψ acceptance. The weight is obtained by successively rotating the event in the angle ψ about the jet-1 axis, checking whether or not such an event would have been accepted, and hence estimating the probability that the original event was observed. The weight is taken as the inverse of this probability. The acceptance criteria were based on full containment within the geometrical acceptance of the detector of three cones centred on the rotated jet axes. The effect on the resulting weights of varying the half-angle defining the size of the cones was studied, and contributes to the systematic error on the result.

7.8 Results

The raw and corrected numbers of events are shown in Table 9 for the various sets of cuts, as discussed above. The values labelled 'σ_3/σ_2' are obtained by dividing the corrected number of 3-jet

8. Conclusions

We have shown that a significant fraction of events triggered on high neutral transverse energy in pp collisions at $\sqrt{s}$ = 62 GeV contain three jets through studies of the shape of the energy flow in each event. The appearance of 2-jet and 3-jet events is clear at ISR energies.

Using a method based on a Fourier analysis of the energy flow the jets have been reconstructed and some of their properties examined. The reconstructed 2-jet events have properties which reproduce those found in an earlier analysis using a more conventional jet-finding algorithm. The two lower-energy jets in 3-jet events tend to lie close together in space, and together recoil against the largest jet. The distribution of separations peaks at small values, consistent with the angular resolution of the reconstruction algorithm, as expected for final-state bremsstrahlung, and inconsistent with phase space.

The momentum of charged particles transverse to the jet axis, j_T, in the jets is constrained below the values from phase space alone, and this is not due to apparatus effects, as expected for bona-fide jets. In particular this is true for the lowest-energy jet in 3-jet events, where within the statistical errors, the j_T is the same as that for jets of the same energy in 2-jet events. The charge ratio formed from the numbers of jets with positive and negative leaders shows values consistent with the expectation that jets in 2-jet events are predominantly due to the fragmentation of u quarks, and that the lowest-energy jet in 3-jet events is due to fragmentation of a neutral parton (gluon).

The projections x_1 and x_2 of the 3-jet Dalitz plot clearly show behaviour characteristic of the l.o. QCD predictions for gluon bremsstrahlung, and disagree with purely phase-space predictions. The angular distribution of the jet axis in 2-jet events also agrees with the QCD expectation. From the ratio of the numbers of 3-jet to 2-jet events measured in our detector we have extracted an estimate for α_S: $\alpha_S(K_3/K_2) = 0.19 \pm 0.02$ (stat.) $\pm$ 0.04 (syst.) at $Q^2 = -\hat{t} \approx 300$ (GeV/c)^2.

Acknowledgements

We would like to acknowledge the contributions of the staff of CERN, notably those in the ISR and DD Divisions, towards the successful completion of this experiment. We particularly thank A. M. Smith, R. Gros, and M.-A. Huber for their assistance.

The following funding agencies have contributed to this experiment: the Department of Energy (U.S.A), the National Science Foundation (U.S.A), and the Science and Engineering Research Council (U.K.).

References

[1] A. L. S. Angelis et al., Phys. Lett. **105B** (1981) 233.

[2] See, e.g., the review talk by G. Wolf, Jet Production and Fragmentation, in Proc. 21st. Int. Conf. on High Energy Physics, J. de Physique, **C-3** (1982) 525.

[3] M. Banner et al., Phys. Lett. **118B** (1982) 203,
G. Arnison et al., Phys. Lett. **123B** (1983) 115.

[4] G. Arnison et al., Phys. Lett. **158B** (1985) 494.

[5] J. A. Appel et al., Z. Phys. C - Particles and Fields **30** (1986) 341.

[6] A. L. S. Angelis et al., Phys. Lett. **126B** (1983) 132.

[7] A. L. S. Angelis et al., Nucl. Phys. **B244** (1984) 1.

[8] T. Åkesson et al., Z. Phys. C. - Particles and Fields **32** (1986) 317.

[9] J. D. Bjorken and S. J. Brodsky, Phys. Rev. **D1** (1970) 1416.

[10] R. Marshall, "Jets and Tests of QCD in e^+e^- Experiments", in Proc. Int. Conf. on High Energy Physics, Lisbon, Portugal, 1981, eds. J. Dias de Deus and J. Soffer, European Physical Society 1982.

[11] A. Donati, R. Odorico, and V. Roberto, "Jet Reconstruction in Collider Events Using Digital Filtering", University of Bologna preprint IFUB 83/13.

[12] F. E. Paige and S. D. Protopopescu, Brookhaven preprint BNL 31987 (1982).

[13] A. L. S. Angelis et al., Nucl. Phys. **B209** (1982) 284.

[14] F. A. Berends, R. Kleiss, P. De Causmaecker, and R. Gastmans, Phys. Lett. **103B** (1981) 124.

[15] T. Gottschalk, E. Monsay, and D. Sivers, Phys. Rev. **D21** (1980) 1799.

[16] Z. Kunstz and E. Pietarinen, Nucl. Phys. **B164** (1980) 45.

[17] F. Halzen and P. Hoyer, Phys. Lett. **130B** (1983) 326.

[18] A recent review is: H.-U. Bengtsson and T. Sjöstrand, "PYTHIA: The Lund Monte Carlo for Hadronic Processes", in the Proceedings of the 1986 Summer Study on the Physics of the Superconducting Supercollider, Snowmass, 1986, eds. R. Donaldson and J. Marx, DPF of the American Physical Society, 1986.

[19] E. Eichten, I. Hinchliffe, K. Lane, and C. Quigg, Rev. Mod. Phys. **56** (1984) 579.

[20] D. W. Duke and J. F. Owens, Phys. Rev. **D30** (1984) 49.

[21] J. C. Collins and D. E. Soper, Phys. Rev. **D16** (1977) 2219.

[22] G. Arnison et al., Phys. Lett. **177B**, 244 (1986).

Table 1: Sphericity comparisons

Class	$<S>$	Fraction of events with:		
		$S<0.1$	$S<0.2$	$S\geq 0.5$
2-jet	0.101 ± 0.001	65%	89%	1%
3-jet	0.261 ± 0.003	14%	45%	10%
>3-jet	0.478 ± 0.004	0.5%	7%	49%

Table 2: Mean jet energies (GeV)

Class	Jet 1	Jet 2	Jet 3
2-jet	16.7	12.3	–
3-jet	14.4	9.9	5.4
>3-jet	10.6	7.5	5.7

Table 3: Mean jet transverse energies (GeV)

Class	Jet 1	Jet 2	Jet 3
2-jet	14.1	10.6	–
3-jet	12.4	8.6	4.5
>3-jet	9.4	6.6	4.9

Table 4: Angular widths (radians)

Class	r.m.s.$\Delta\phi_{12}$	$<\alpha_{12}>$	$<\alpha_{23}>$
2-jet	0.22	2.62	–
3-jet	0.55	2.46	1.47
>3-jet	1.10	2.14	1.62

Table 5: *Coefficients from integrated l.o. QCD cross sections with loosest cuts:*

3-jet: $x_1 \leq 0.92$, $|\cos\theta_1| \leq 0.4$, $45° < \psi < 145°$;
2-jet: $|\cos\theta| \leq 0.6$ (see text for details).

Subprocess	C_3	C_2	C_3/C_2
gg	46.6	45.2	1.031
qg	14.5	19.1	0.759
qq	3.65	6.15	0.593
qq′	4.58	7.44	0.616

Table 6: *Coefficients from integrated l.o. QCD cross sections with cuts:*

3-jet: $x_1 \leq 0.90$, $|\cos\theta_1| \leq 0.3$, $50° < \psi < 130°$;
2-jet: $|\cos\theta| \leq 0.5$ (see text for details).

Subprocess	C_3	C_2	C_3/C_2
gg	20.6	32.0	0.644
qg	6.26	13.3	0.471
qq	1.52	4.05	0.375
qq′	1.99	5.08	0.392

Table 7: *Coefficients from integrated l.o. QCD cross sections with tightest cuts:*

3-jet: $x_1 \leq 0.90$, $|\cos\theta_1| \leq 0.4$, $60° < \psi < 120°$;
2-jet: $|\cos\theta| \leq 0.3$ (see text for details).

Subprocess	C_3	C_2	C_3/C_2
gg	9.10	15.7	0.580
qg	2.66	6.41	0.415
qq	0.597	1.80	0.332
qq′	0.812	2.37	0.343

Table 8: Mean jet energies (GeV) in rest frame

Class	Jet 1	Jet 2	Jet 3
2-jet	13.7	13.4	–
3-jet	12.7	9.9	5.4

Table 9: *Numbers of events and resulting value of α_s :*

Each sample is defined by the cut set [2-jet max(|Cos θ|), 3-jet max(|Cos θ|),min(ψ),max(x_1)]; The acceptance-corrected no. of 3-jet events appears in parentheses; (See text for more details).

Sample	3-jets	2-jets	σ_3/σ_2	$< C_3/C_2 >$	$\alpha_S(K_3/K_2)$
[0.6, 0.4,45,0.92]	181 (259.7)	2090	0.124±0.010	0.723	0.172±0.014
[0.6, 0.4,45,0.90]	143 (199.8)	2090	0.096±0.008	0.552	0.174±0.015
[0.5, 0.3,50,0.92]	121 (169.4)	1622	0.104±0.010	0.593	0.175±0.017
[0.5, 0.3,50,0.90]	98 (136.2)	1622	0.084±0.009	0.453	0.185±0.020
[0.5, 0.3,60,0.90]	65 (86.8)	1622	0.054±0.007	0.301	0.179±0.023
[0.3, 0.2,60,0.90]	40 (57.6)	824	0.070±0.010	0.402	0.174±0.027
[0.4, 0.2,60,0.90]	40 (57.6)	1187	0.049±0.008	0.273	0.179±0.029
[0.5, 0.2,60,0.90]	40 (57.6)	1622	0.036±0.006	0.190	0.189±0.032

Figure Captions

Fig. 1: View of R110 detector along ISR beams.

Fig. 2: Dalitz plot representation of the data in terms of the Q_1, Q_2, Q_3 parameters defined in the text:

a) Axes of the Dalitz plot, with the shaded area showing the physically-populated region (due to the Q_i ordering);

b) The Dalitz plot for the data;

c) Projection of data on the Sphericity axis;

d) Projection of data on the $(\sqrt{3}/2)(Q_2 - Q_1)$ axis.

Fig. 3: The distribution of normalized energy flow, $(1/E_{tot})(dE/d\phi)$, as a function of ϕ, an azimuthal angle defined relative to the S-axis (a,b, and c), or to the highest-energy jet (d), for

a) "Raw data": all events;

b) "2-jet-like": events of class a) with $Q_1 < 0.05$, $Q_2 < 0.05$;

c) "Planar, broad recoil": events of class a) with $Q_1 < 0.1$, $(Q_2 - Q_1) > 0.1$;

d) Events with exactly 3 reconstructed jets.

Fig. 4: The size of the energy smearing as a function of the parameters used in the filter functions (see text).

Fig. 5: Typical energy distributions within the detector, represented by a tower proportional to the energy deposition in each cell of a grid (θ,ϕ) for:

a) a 2-jet event;

b) a 3-jet event;

c) an event with more than 3 jets;

d) 2-jet event a) after filtering;

e) 3-jet event b) after filtering;

f) event c) after filtering.

Fig. 6: The fraction of events with exactly two, three, or more than three jets as a function of E^0_{tot}, the total neutral energy in the event.

Fig. 7: The numbers of events with two, three, and four jets having total invariant masses above 20 GeV/c^2, as a function of the total neutral energy in the events.

Fig. 8: The numbers of jets reconstructed in the data, as a function of the minimum cut-off energy required to define a jet.

Fig. 9: The efficiency of the algorithm in resolving two jets, as a function of the angular separation between the jets. The standard filter parameters are $(\alpha_1,\alpha_2)=(0.55,0.25)$, and these values reduced by a factor of two are $(\alpha_1,\alpha_2)=(0.275,0.125)$.

Fig. 10: The mean angular separation, α_{23}, between the two lowest-energy reconstructed jets, as a function of the α_{23} between the original parton directions in 3-jet ISAJET Monte Carlo events.

Fig. 11: The energy spectrum of the lowest-energy jet in events with exactly three jets.

Fig. 12: Distribution of angular separation, α_{23}, between the two lower-energy jets in events with exactly three jets. The solid line represents a phase-space distribution (see text).

Fig. 13: Mean value of charged-particle transverse momentum j_T, w.r.t. the jet axis, as a function of the fragmentation z, for the lowest-energy jet in 3-jet events. Note the suppressed-zero scale.

a) j_T for the lowest-energy jet in real and random (see text) 3-jet events.

b) j_T for the lowest-energy jet in 3-jet events, and for the jets in 2-jet events from $\pi^0\pi^0$ events.

c) j_T for the lowest-energy jet in fake 3-jet events, and for the jets in fake 2-jet events, both for the E_{jet} range $4-8$ GeV and with $<E_{jet}>$ = 5.8 GeV. The ratio of the curves is also shown.

Fig. 14: Mean charge asymmetry for leading particles in jets as a function of z. The solid curve is the prediction from ISAJET for a mixture of fragmenting u-quarks and d-quarks in the ratio 2:1. (The ISAJET prediction for gluon fragmentation is zero).

a) For jets 1 and 2 in 2-jet events (over the E_{jet} range $8-28$ GeV), and for jet 3 in 3-jet events (E_{jet} $4-8$ GeV);

b) For jet 3 in 3-jet events (E_{jet} $4-8$ GeV) and for the lower-energy jet in 2-jet $\pi^0\pi^0$ events (also E_{jet} $4-8$ GeV).

Fig. 15: System of axes used to specify 3-jet events.

Fig. 16: Ratio of numbers of 3-jet and 2-jet events as a function of the invariant mass of the three or two highest-energy jets in the events.

Fig. 17: Typical Dalitz plot (x_2 vs x_1) representation of a sample of 3-jet events selected by $M \geq 20$ GeV/c^2, $\Sigma E^0_{jet} \geq 19$ GeV, and [0.5,0.3,50,0.92] (using the notation of Tables 9). The solid lines represent typical l.o. QCD predictions (for 64% $qq \rightarrow qqg$ + 36% $qg \rightarrow qgg$); the dashed lines represent what is expected from phase space alone.

a) x_2 vs x_1;

b) Projection onto x_1 axis;

c) Projection onto x_2 axis.

Fig. 18: Angular distribution of jet-axis in a sample of 2-jet events, normalized to 1.0 at $|\text{Cos}\ \theta| = 0$. The solid curve is the QCD prediction for a mix of 64% $qq \rightarrow qq$ + 36% $qg \rightarrow qg$.

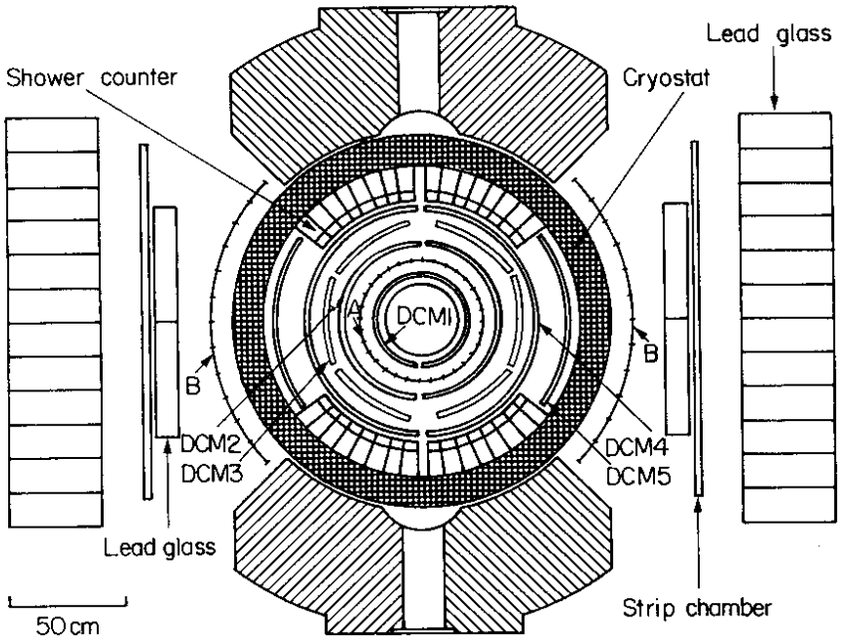
Lead glass
Shower counter
Cryostat
DCM1
A
B
B
DCM2
DCM3
DCM4
DCM5
Lead glass
Strip chamber
50 cm

Fig. 1

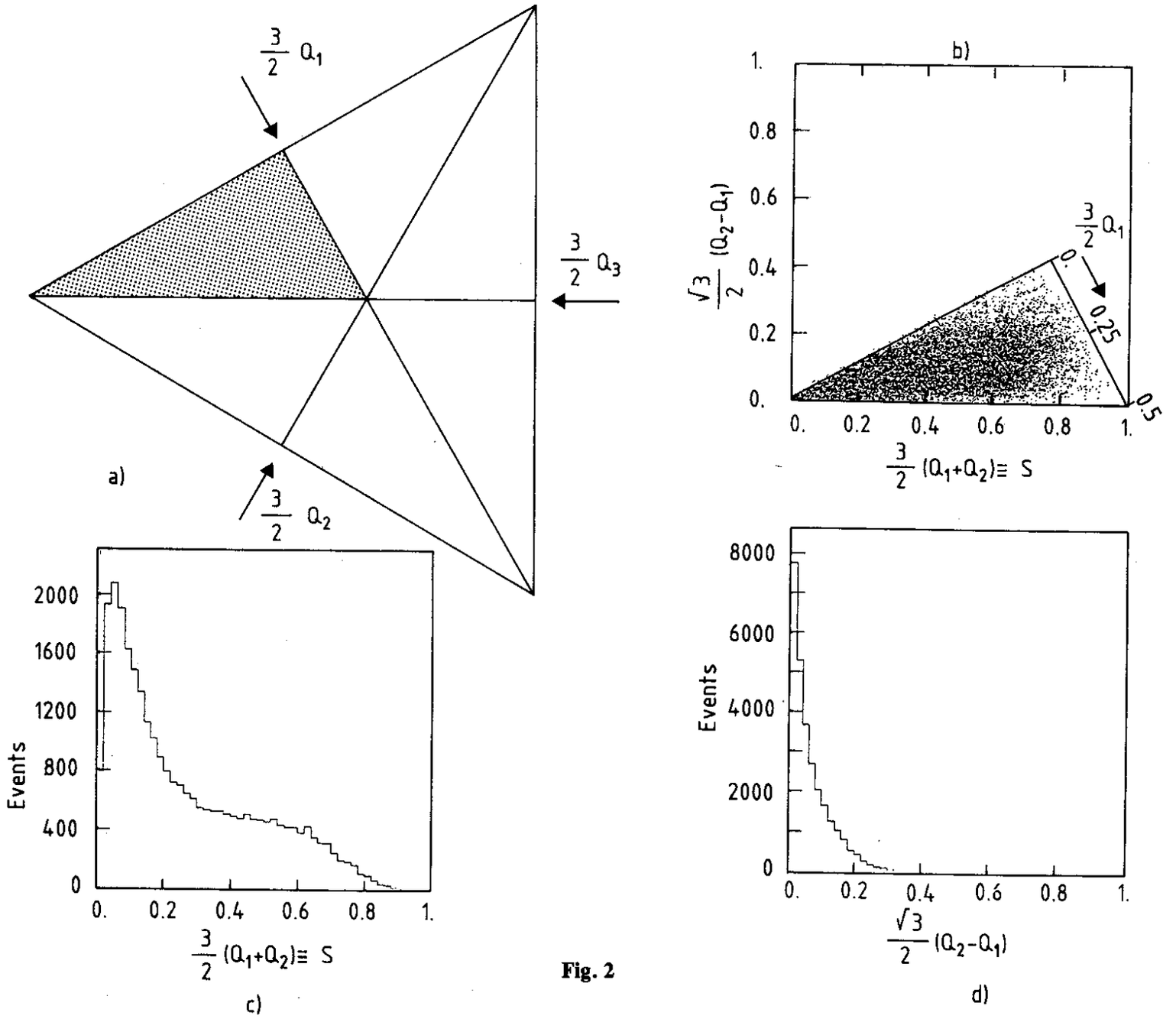
$\frac{3}{2}Q_1$
$\frac{3}{2}Q_3$
$\frac{3}{2}Q_2$
a)
b)
$\frac{\sqrt{3}}{2}(Q_2-Q_1)$
$\frac{3}{2}(Q_1+Q_2)\equiv S$
0.
0.25
0.5
c)
Events
$\frac{3}{2}(Q_1+Q_2)\equiv S$
d)
Events
$\frac{\sqrt{3}}{2}(Q_2-Q_1)$

Fig. 2

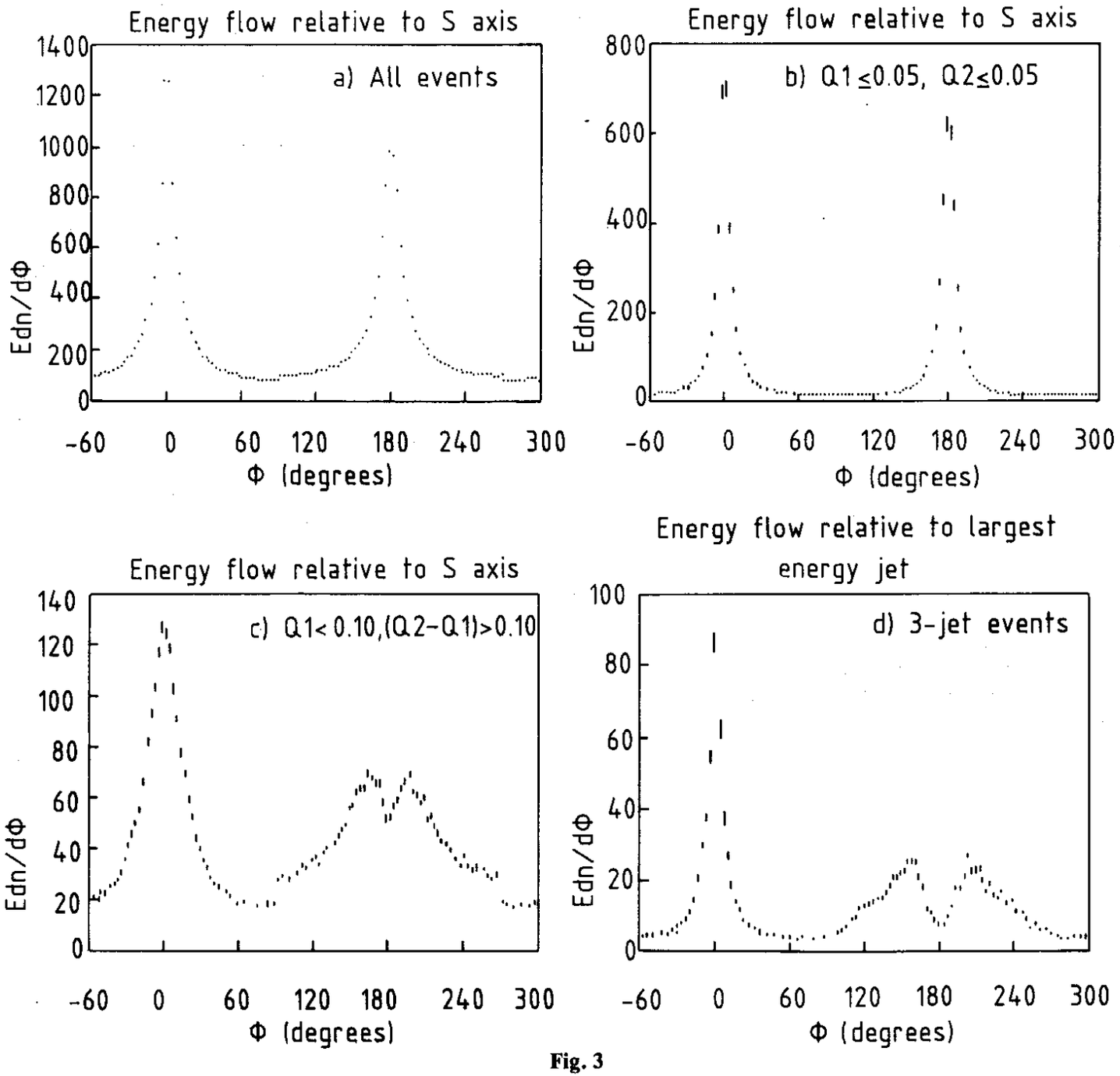
Energy flow relative to S axis
a) All events
Edn/dΦ
Φ (degrees)
Energy flow relative to S axis
b) Q1≤0.05, Q2≤0.05
Edn/dΦ
Φ (degrees)
Energy flow relative to S axis
c) Q1< 0.10,(Q2-Q1)>0.10
Edn/dΦ
Φ (degrees)
Energy flow relative to largest energy jet
d) 3-jet events
Edn/dΦ
Φ (degrees)

Fig. 3

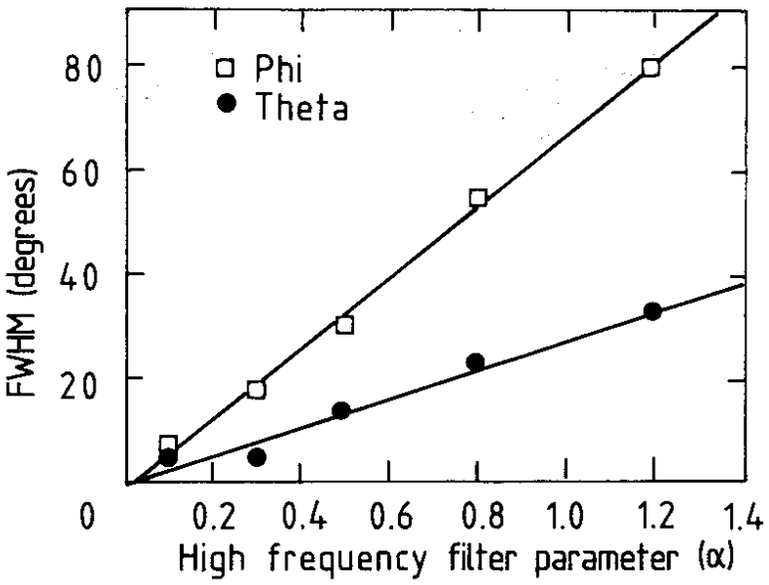
Phi
Theta
FWHM (degrees)
0
20
40
60
80
0.2
0.4
0.6
0.8
1.0
1.2
1.4
High frequency filter parameter (α)

Fig. 4

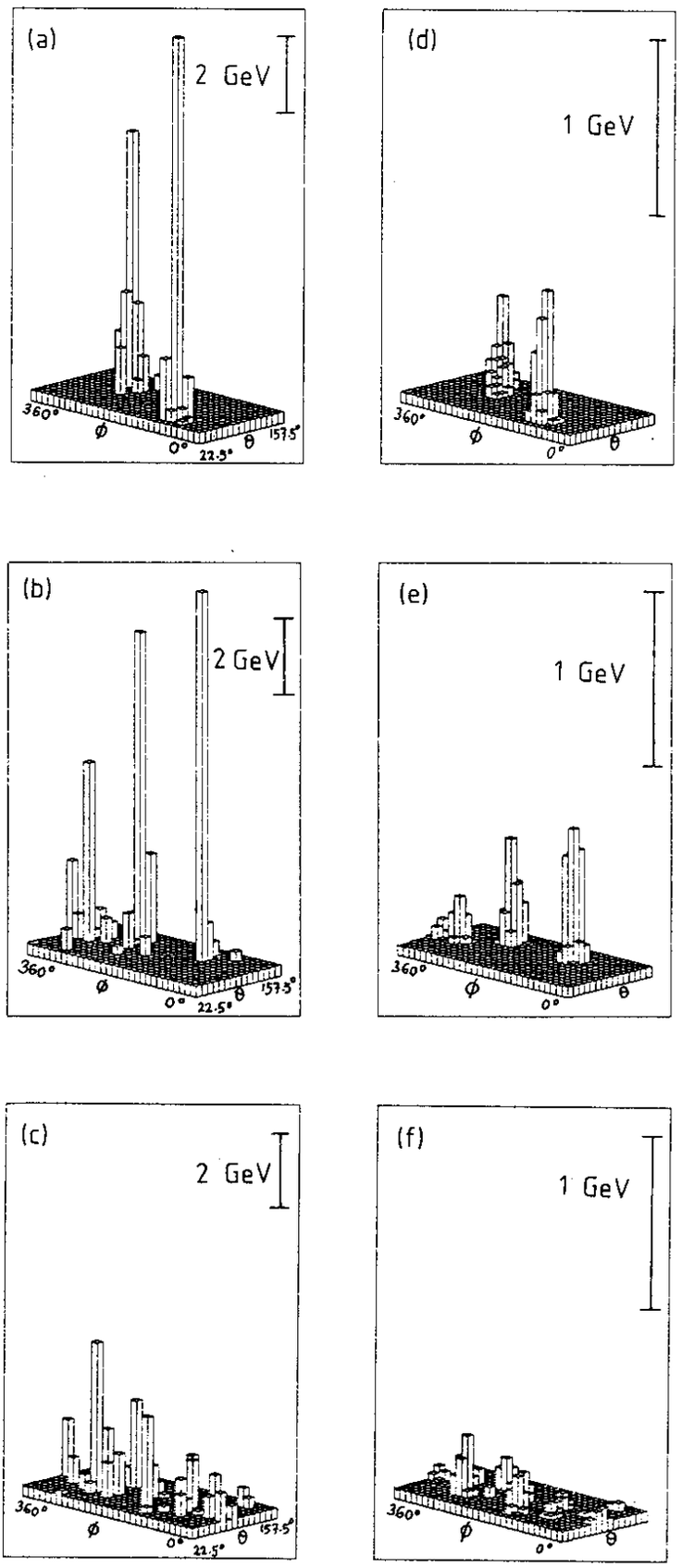
(a)
2 GeV
360°
φ
0°
22.5°
θ
157.5°
(d)
1 GeV
360°
φ
0°
θ
(b)
2 GeV
360°
φ
0°
22.5°
θ
157.5°
(e)
1 GeV
360°
φ
0°
θ
(c)
2 GeV
360°
φ
0°
22.5°
θ
157.5°
(f)
1 GeV
360°
φ
0°
θ

Fig. 5

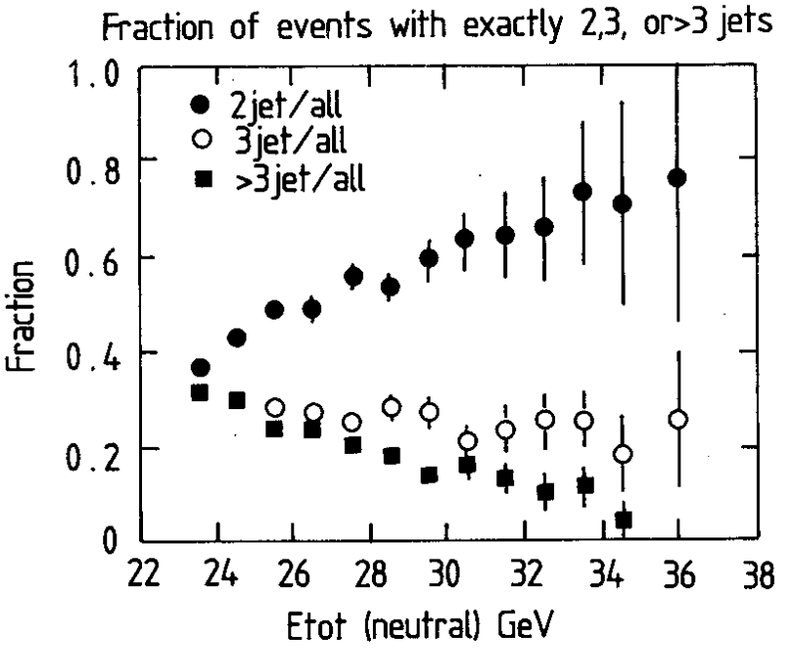
Fraction of events with exactly 2,3, or>3 jets
1.0
0.8
0.6
0.4
0.2
0
Fraction
2jet/all
3jet/all
>3jet/all
22
24
26
28
30
32
34
36
38
Etot (neutral) GeV

Fig. 6

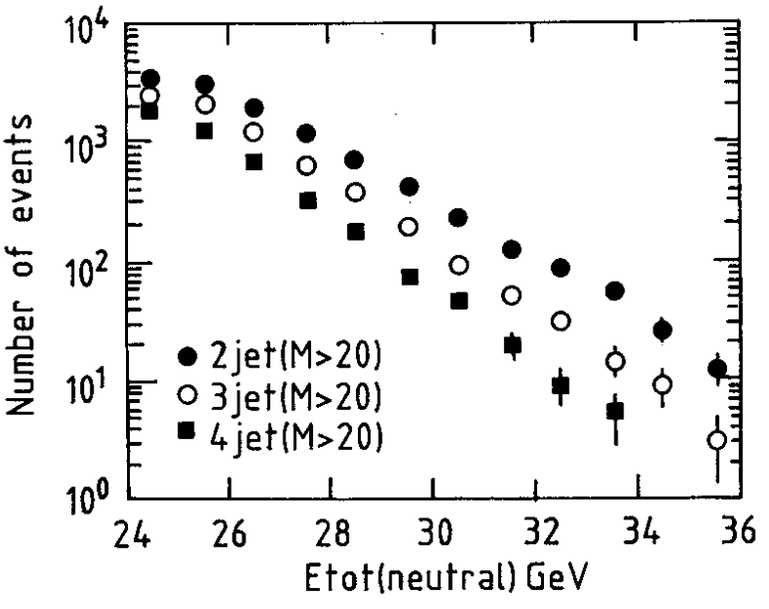
10^4
10^3
10^2
10^1
10^0
Number of events
2jet(M>20)
3jet(M>20)
4jet(M>20)
24
26
28
30
32
34
36
Etot(neutral) GeV

Fig. 7

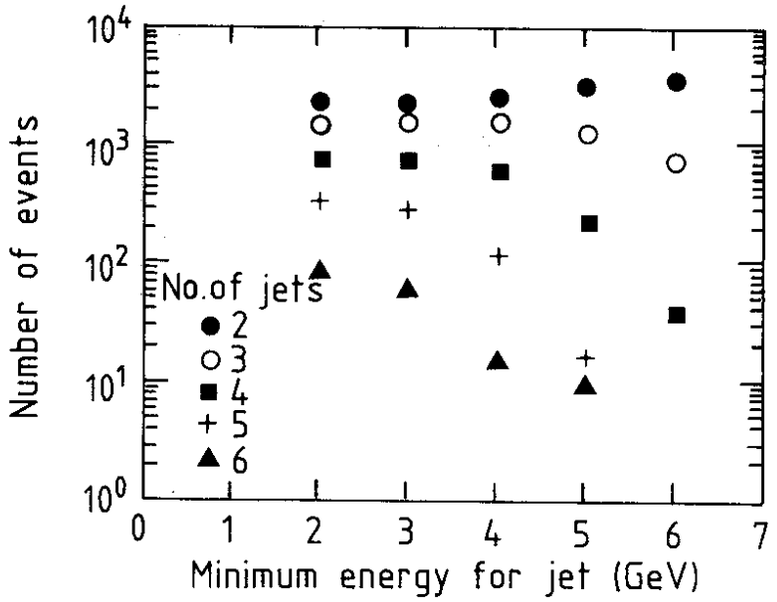
Number of events
10^4
10^3
10^2
10^1
10^0
No.of jets
2
3
4
5
6
0 1 2 3 4 5 6 7
Minimum energy for jet (GeV)

Fig. 8

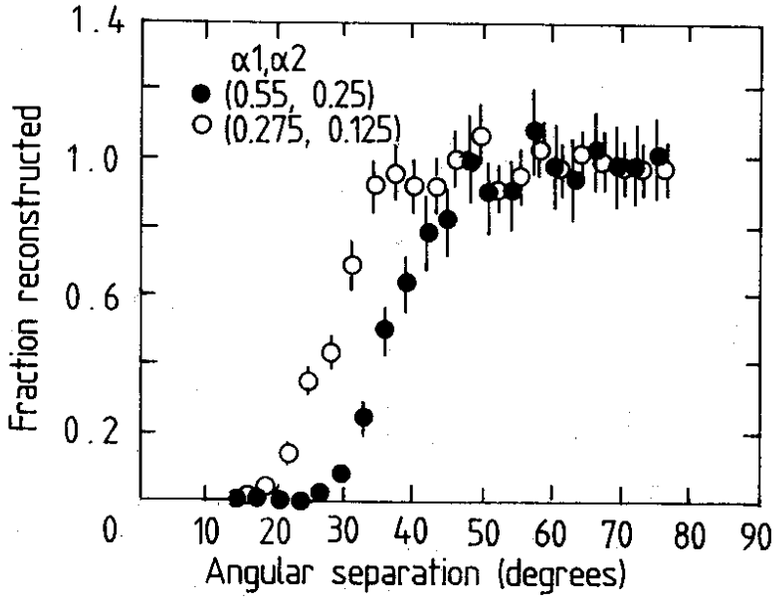
Fraction reconstructed
1.4
1.0
0.6
0.2
0
α1,α2
(0.55, 0.25)
(0.275, 0.125)
10 20 30 40 50 60 70 80 90
Angular separation (degrees)

Fig. 9

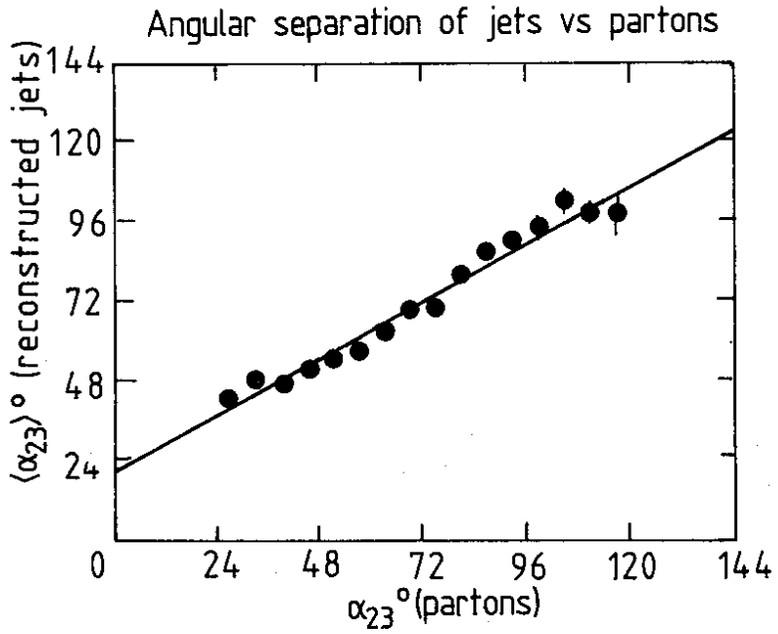
Angular separation of jets vs partons
⟨α23⟩° (reconstructed jets)
144
120
96
72
48
24
0
24
48
72
96
120
144
α23°(partons)

Fig. 10

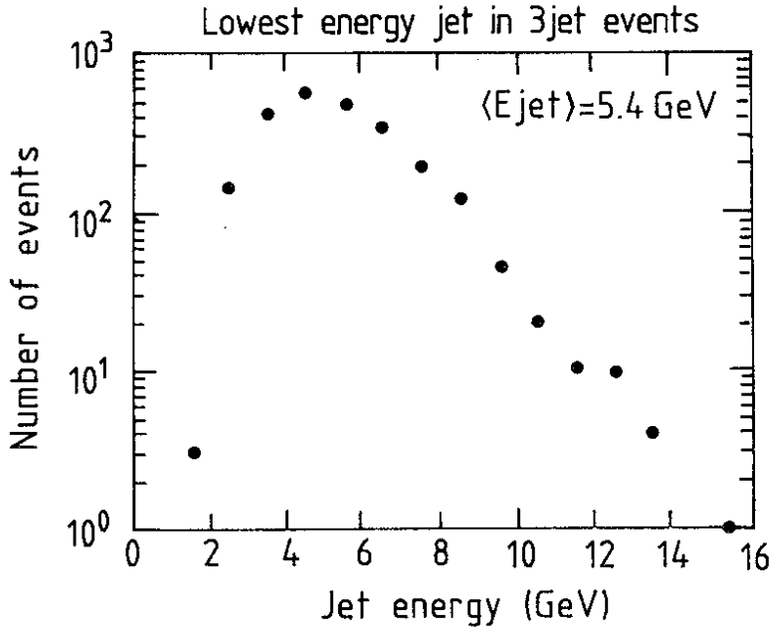
Lowest energy jet in 3jet events
⟨Ejet⟩=5.4 GeV
Number of events
10³
10²
10¹
10⁰
0
2
4
6
8
10
12
14
16
Jet energy (GeV)

Fig. 11

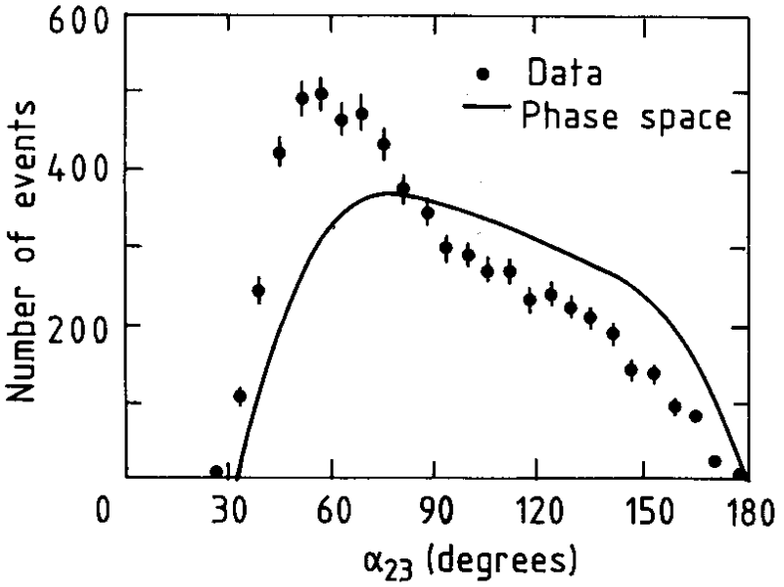
600
400
200
0
30
60
90
120
150
180
Number of events
Data
Phase space
α_{23} (degrees)

Fig. 12

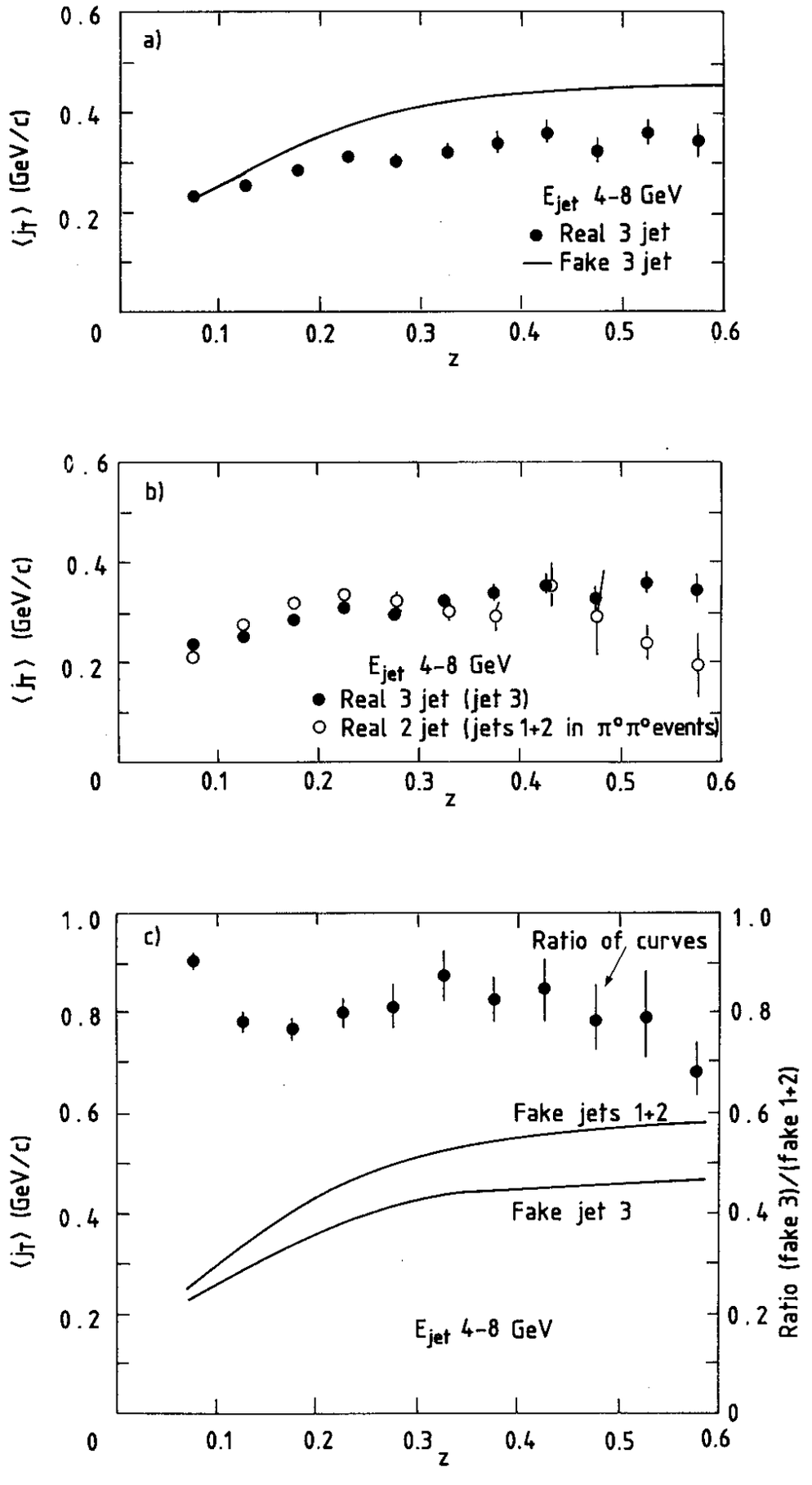
a)
E_{jet} 4-8 GeV
Real 3 jet
Fake 3 jet
$\langle j_T \rangle$ (GeV/c)
z
b)
E_{jet} 4-8 GeV
Real 3 jet (jet 3)
Real 2 jet (jets 1+2 in $\pi^0\pi^0$ events)
$\langle j_T \rangle$ (GeV/c)
z
c)
Ratio of curves
Fake jets 1+2
Fake jet 3
E_{jet} 4-8 GeV
$\langle j_T \rangle$ (GeV/c)
Ratio (fake 3)/(fake 1+2)
z

Fig. 13

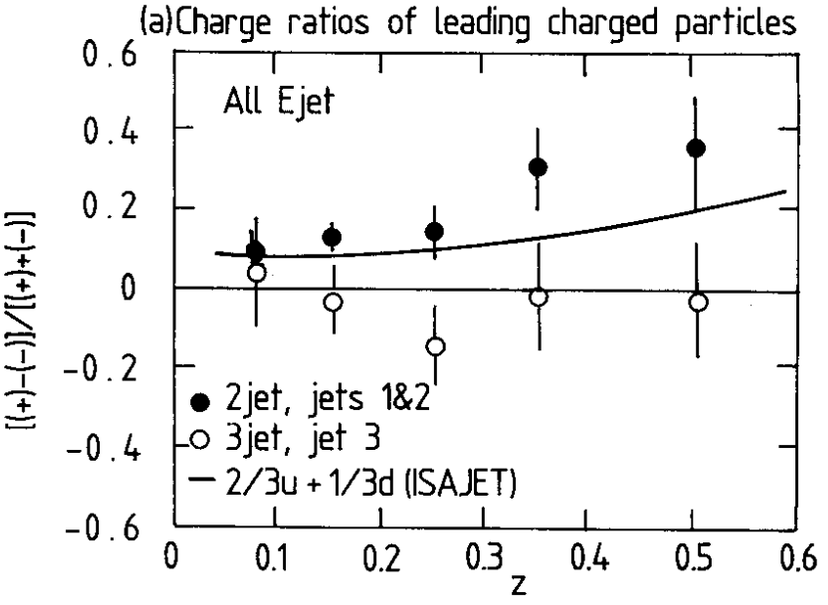
(a)Charge ratios of leading charged particles
All Ejet
2jet, jets 1&2
3jet, jet 3
2/3u + 1/3d (ISAJET)
[(+)-(-)]/[(+)+(-)]
z

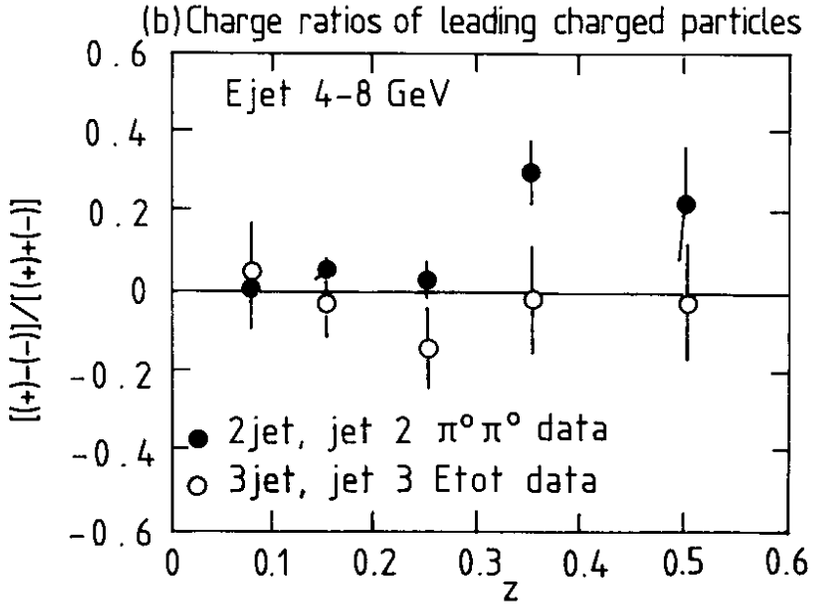
(b)Charge ratios of leading charged particles
Ejet 4-8 GeV
2jet, jet 2 π°π° data
3jet, jet 3 Etot data
[(+)-(-)]/[(+)+(-)]
z

Fig. 14

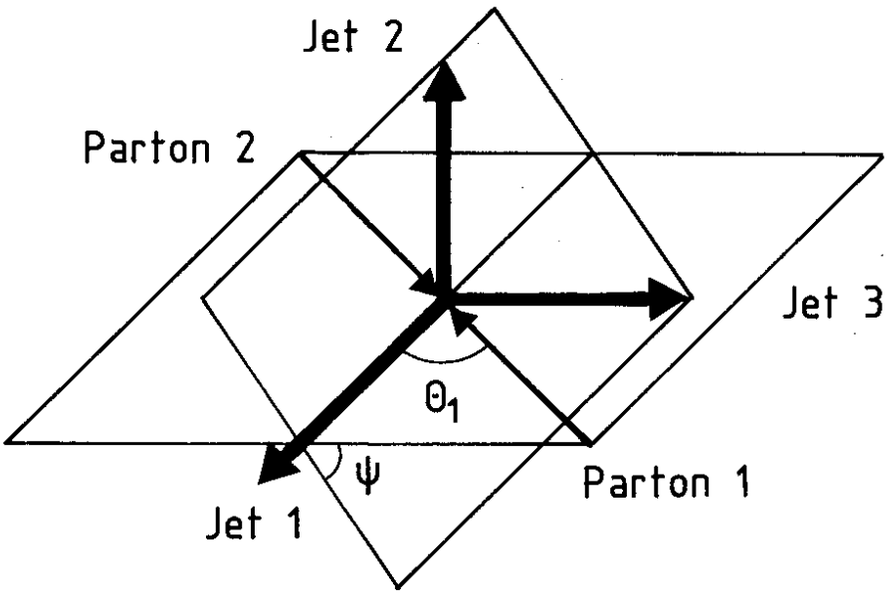
Jet 2
Parton 2
Jet 3
Θ_1
ψ
Parton 1
Jet 1

Fig. 15

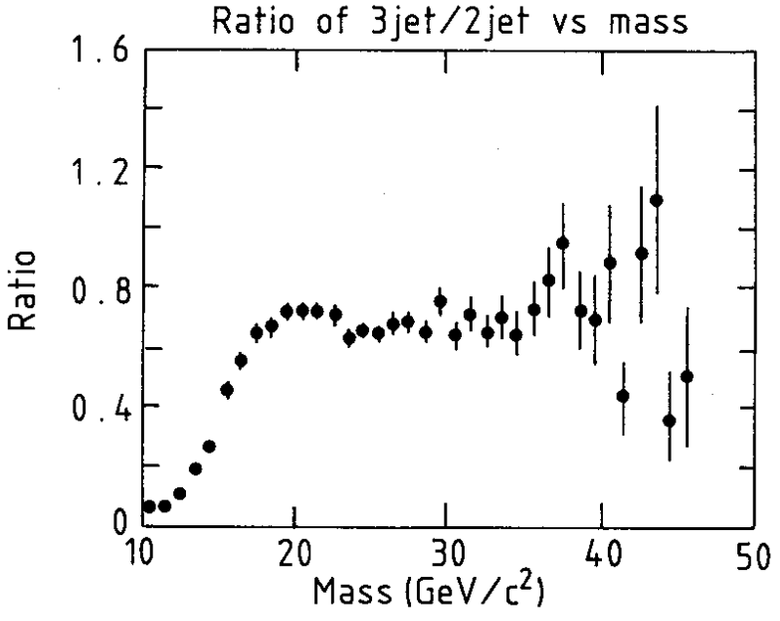
Ratio of 3jet/2jet vs mass
Ratio
1.6
1.2
0.8
0.4
0
10
20
30
40
50
Mass (GeV/c^2)

Fig. 16

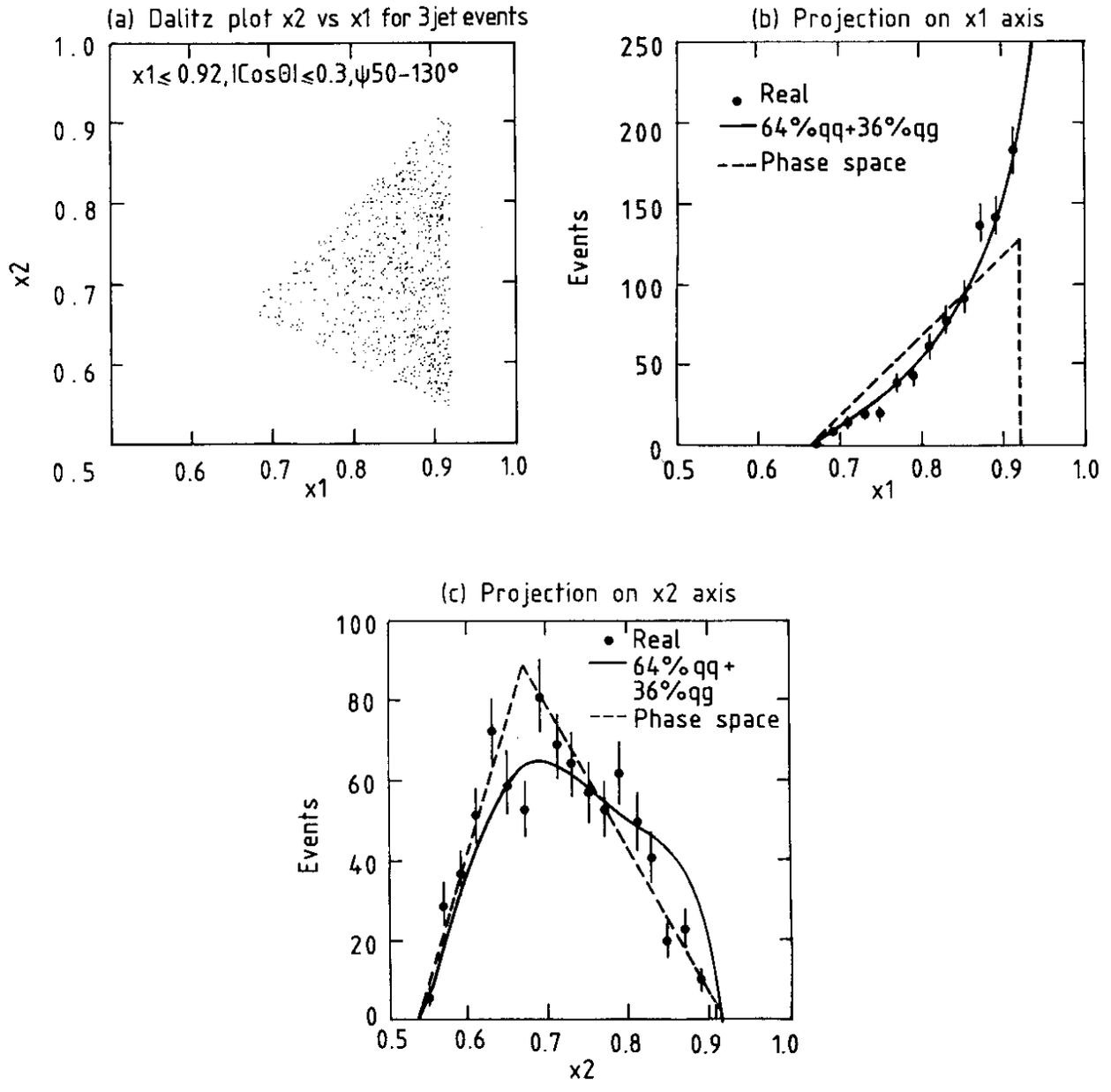
(a) Dalitz plot x2 vs x1 for 3jet events
x1≤ 0.92, |Cosθ|≤0.3, ψ50-130°
x2
x1
(b) Projection on x1 axis
Real
64%qq+36%qg
Phase space
Events
x1
(c) Projection on x2 axis
Real
64% qq +
36%qg
Phase space
Events
x2

Fig. 17

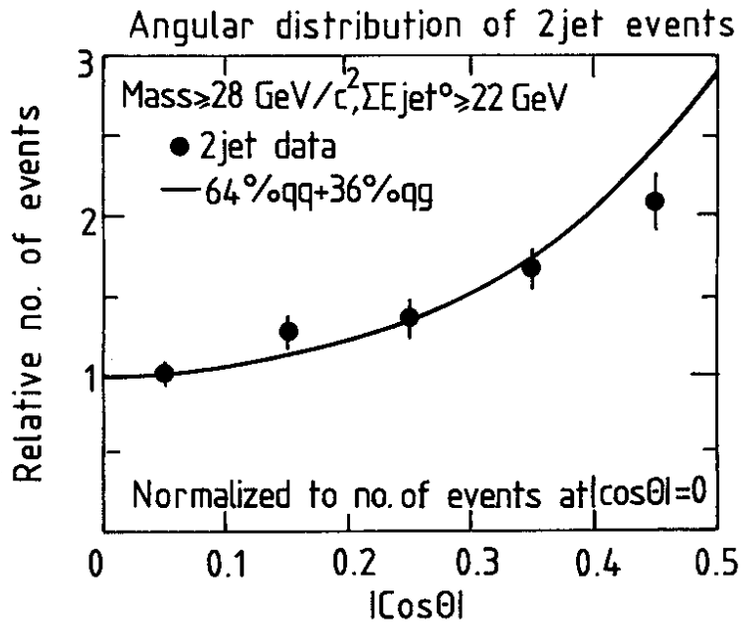
Angular distribution of 2jet events
Mass≥28 GeV/c²,ΣEjet°≥22 GeV
● 2jet data
—64%qq+36%qg
Normalized to no. of events at |cosΘ|=0
Relative no. of events
|CosΘ|
0
0.1
0.2
0.3
0.4
0.5
1
2
3

Fig. 18